Cellular/Molecular

T-Type Ca^{2+} Channels Boost Neurotransmission in Mammalian Cone Photoreceptors

Adam Davison,* Uwe Thorsten Lux,* Johann Helmut Brandstätter, and Norbert Babai
Department of Biology, Animal Physiology/Neurobiology, Friedrich-Alexander-Universität Erlangen-Nürnberg, 91058 Erlangen, Germany

It is a commonly accepted view that light stimulation of mammalian photoreceptors causes a graded change in membrane potential instead of developing a spike. The presynaptic Ca^{2+} channels serve as a crucial link for the coding of membrane potential variations into neurotransmitter release. $Ca_v1.4$ L-type Ca^{2+} channels are expressed in photoreceptor terminals, but the complete pool of Ca^{2+} channels in cone photoreceptors appears to be more diverse. Here, we discovered, employing whole-cell patch-clamp recording from cone photoreceptor terminals in both sexes of mice, that their Ca^{2+} currents are composed of low- (T-type Ca^{2+} channels) and high- (L-type Ca^{2+} channels) voltage-activated components. Furthermore, Ca^{2+} channels exerted self-generated spike behavior in dark membrane potentials, and spikes were generated in response to light/dark transition. The application of fast and slow Ca^{2+} chelators revealed that T-type Ca^{2+} channels are located close to the release machinery. Furthermore, capacitance measurements indicated that they are involved in evoked vesicle release. Additionally, RT-PCR experiments showed the presence of $Ca_v3.2$ T-type Ca^{2+} channels in cone photoreceptors but not in rod photoreceptors. Altogether, we found several crucial functions of T-type Ca^{2+} channels, which increase the functional repertoire of cone photoreceptors. Namely, they extend cone photoreceptor light-responsive membrane potential range, amplify dark responses, generate spikes, increase intracellular Ca^{2+} levels, and boost synaptic transmission.

Key words: **calcium; $Ca_v3.2$; cone photoreceptors; exocytosis; spike**

Significance Statement

Photoreceptors provide the first synapse for coding light information. The key elements in synaptic transmission are the voltage-sensitive Ca^{2+} channels. Here, we provide evidence that mouse cone photoreceptors express low-voltage-activated $Ca_v3.2$ T-type Ca^{2+} channels in addition to high-voltage-activated L-type Ca^{2+} channels. The presence of T-type Ca^{2+} channels in cone photoreceptors appears to extend their light-responsive membrane potential range, amplify dark response, generate spikes, increase intracellular Ca^{2+} levels, and boost synaptic transmission. By these functions, $Ca_v3.2$ T-type Ca^{2+} channels increase the functional repertoire of cone photoreceptors.

Introduction

In the outer segment of cone photoreceptors, incident light is absorbed by photopigments, which trigger phototransduction and generate a photocurrent (Baylor et al., 1987; Schnapf et al., 1987). The photocurrent is further processed at the inner segment by voltage-sensitive channels (Barnes and Hille, 1989; Barnes, 1994) to generate photovoltage at the cone photoreceptor synaptic terminal. Previously identified voltage-gated channels of cone photoreceptors are the delayed rectifier K^+ channels, the fast transient K^+ channels, the hyperpolarization-activated cation channels, and the high-voltage-activated L-type Ca^{2+} channels (Barnes and Hille, 1989; Maricq and Korenbrot, 1990; Yagi and Macleish, 1994; Schneeweis and Schnapf, 1995; Gayet-Primo et al., 2018). Based on the repertoire of the expressed voltage-sensitive ion channels, it is generally believed that depolarization of the cone photoreceptor membrane does not result in spiking behavior, but rather in a gradual potential change (Barnes and Hille, 1989; Yagi and Macleish, 1994; Schneeweis and Schnapf, 1995; Masland, 2012). On the other hand, there is physiological evidence for fast, spike-like currents in monkey rod photoreceptors (Schnapf et al., 1990). Additionally, Na^+ action potentials were also described in human cone and rod photoreceptors from detached retinal tissue (Kawai et al., 2001, 2005), but there is no evidence for Na^+ action potentials in healthy, uncompromised photoreceptors.

Electrophysiological studies have shown the presence of high-voltage-activated (HVA) L-type Ca^{2+} channels, but not of other

Received Sep. 16, 2021; revised June 13, 2022; accepted June 22, 2022.

Author contributions: J.H.B. and N.B. designed research; A.D., U.T.L., and N.B. performed research; A.D., U.T.L., and N.B. analyzed data; N.B. wrote the paper.

This work was supported by the "Deutsche Forschungsgemeinschaft" (Grant BA 6688/1-1). We thank Dr. Andreas Gießl for helpful advice in performing PCR experiments on sorted cells. Furthermore, we thank Andrea Nerz and Beata Schmidt for excellent technical assistance.

*A.D. and U.T.L. contributed equally to this work and should be considered as joint first authors.

The authors declare no competing financial interests.

Correspondence should be addressed to Norbert Babai at norbert.babai@fau.de.

https://doi.org/10.1523/JNEUROSCI.1878-21.2022

types of Ca^{2+} channels, in cone photoreceptors of multiple species (Barnes and Hille, 1989; Lasater and Witkovsky, 1991; Wilkinson and Barnes, 1996). Immunocytochemical labeling of the outer plexiform layer of the retina with antibodies against the pore-forming subunits of the HVA $Ca_v1.3$ (α1D) and $Ca_v1.4$ (α1F) channels indicated the existence of both Ca^{2+} channel types in photoreceptors (Nachman-Clewner et al., 1999; Morgans, 2001; Morgans et al., 2001; Specht et al., 2009; Kersten et al., 2010). Antibodies against $Ca_v1.3$ labeled a subtype of cone photoreceptors in the tree shrew retina, which were probably the middle wavelength-sensitive ones (Taylor and Morgans, 1998; Morgans, 1999). Immunoelectron microscopy also suggested the presence of $Ca_v1.3$ channels in mouse cone photoreceptor synaptic terminals (Kersten et al., 2010), but the ERG b-wave was not altered in a mutant $Ca_v1.3$ mouse model (Wu et al., 2007). By contrast, experiments using a mutant $Ca_v1.4$ mouse model show a dramatically reduced ERG b-wave, and in humans, the mutation of the $Ca_v1.4$ channel causes congenital stationary night blindness. This demonstrates that the main Ca^{2+} channel of photoreceptors is $Ca_v1.4$ (Strom et al., 1998; Mansergh et al., 2005). However, a $Ca_v1.4$ mutation in mouse cone photoreceptors did not significantly change tonic synaptic vesicle release (Zanetti et al., 2021), indicating the presence of another, possibly non-L-type voltage-sensitive Ca^{2+} channel, in cone photoreceptors.

The voltage dependence of Ca^{2+} channels in cone photoreceptors of nonmammalian vertebrates is considered to be similar to that in rod photoreceptors (Bader et al., 1982; Kaneko and Tachibana, 1986). Additionally, previous electrophysiological measurements of cone photoreceptor Ca^{2+} currents (I_{Ca}) in mice showed a similar voltage dependence to rod photoreceptors (Hirano et al., 2016; Babai et al., 2019; Grassmeyer et al., 2019). Whole-cell patch-clamp recordings of cone photoreceptors usually target the cell bodies or inner segments, which are separated from the synaptic terminals by a relatively long axon. In previous works, the signal flow through cone photoreceptor axons showed a short (Lasater et al., 1989) and also a long (Bryman et al., 2020) length constant in turtle and macaque retina, respectively. As the length constant is not determined in mouse cone photoreceptors, the anatomic arrangement may limit electrical access to voltage-gated channels at the synapse where voltage-gated Ca^{2+} channels are clustered (Xu and Slaughter, 2005; Choi et al., 2008; Mercer et al., 2011). In this study, we characterized the voltage dependence of mouse cone photoreceptor I_{Ca} by recording directly from their synaptic terminals using low-resistance (~10 MΩ) patch pipettes.

Materials and Methods

Mice. Adult (age, 2–5 months) male and female C57BL/6 mice (The Jackson Laboratory) and Tg(Rac3-EGFP)JZ58Gsat/Mmcd (Rac3-eGFP; Landgraf et al., 2012; Regus-Leidig et al., 2013) mice were used for the electrophysiological and fluorescence-activated cell sorting (FACS) experiments. Rac3-eGFP mice, expressing enhanced green fluorescent protein (eGFP) in all cone photoreceptor cells were used. These mice were obtained from the Mutant Mouse Regional Resource Center (MMRRC), a National Center for Research Resources-NIH-funded strain repository and were donated to the MMRRC by the National Institute of Neurological Disorders and Stroke-funded GENSAT (Gene Expression Nervous System Atlas) BAC Transgenics Project. The Rac3-eGFP construct was generated by inserting an eGFP reporter gene, followed by a polyadenylation sequence, into the bacterial artificial chromosome (BAC) clone RP23-62A17 at the initiating ATG codon of the first coding exon of the Rac3 gene. Consequently, eGFP expression was driven by the regulatory sequence of the Rac3 gene. The resulting modified BAC (BX1967) was used to isolate the transgene. The animals were kept in a 12 h light/dark cycle. All experiments were performed in compliance with the guidelines for the welfare of experimental animals issued by the Federal Government of Germany and the University of Erlangen-Nürnberg.

Table 1. Primer pairs used for RT-PCR

Primer	Sequence
LVA (degenerated) forward	5′ GT(AG)GA(AG)GG(CT)TTCCAGGC(AGT)GAGG 3′
LVA (degenerated) reverse	5′-GCTGTTCC(AG)GCTGGAGCG(AGC)C 3′
$Ca_v3.1$ forward	5′-CACCAAGTCTGAGTCAGAGC-3′
$Ca_v3.1$ reverse	5′-TGATTTCATCTCATGATGGGC-3′
$Ca_v3.2$ forward	5′-AGAGGAAGATTTCGATAAGCT-3′
$Ca_v3.2$ reverse	5′-GGCTGCTTCCTGCTCTGTT-3′
$Ca_v3.3$ forward	5′-AAGCTCC(AC)(AG)GA(AG)GGCCTGGA-3′
$Ca_v3.3$ reverse	5′-GTAGTAGGAGCTCCGGGAGCT-3′
Actb forward	5′-TTCCTCCCTGGAGAAGAG-3′
Actb reverse	5′-CACTGTGTTGGCATAGAG-3′
Opn1sw forward	5′-CTCTTCTGCATCTTCTCT-3′
Opn1sw reverse	5′-AGGGTTTACAGATGACAA-3′
Rho forward	5′-GTCATCTACATCATGTTGAAC-3′
Rho reverse	5′-ATCTCCCAGTGGATTCTT-3′

Primers for LVA T-type Ca^{2+} channels adapted from Vignali et al. (2006).

Fluorescence-activated cell sorting of photoreceptors. For sorting of photoreceptors, retinae of Rac3-eGFP mice were dissociated by papain digestion (10 U/ml; Worthington Biochemical) at 37°C for 20 min and subsequent trituration. After washing with FACS buffer (5 mM EDTA in 0.1 M PBS), pH 7.4, the dissociated cells were treated with RNase A (0.9 U; Carl Roth) in FACS buffer at 37°C for 5 min, for degrading the RNA of damaged cells. After DAPI wash, the cells were resuspended in FACS buffer with RiboLock RNase inhibitor (20 U; Thermo Fisher Scientific) for inhibiting remaining RNase activity. Cells were sorted in a FACS Aria III (BD Biosciences) with an 85 µm nozzle at the Chair of Genetics, Friedrich-Alexander University Erlangen-Nürnberg and directly collected in RLT Buffer (Qiagen) containing 1% β-mercaptoethanol. Cone photoreceptors were sorted by cone-specific fluorescence of Rac3-eGFP mice. Rod photoreceptors were sorted by forward and sideward scatter in an approach adapted from Feodorova et al. (2015). The population identified by forward scatter (FSC)/sideward scatter (SSC) was positive for CD73, a surface marker of cone/rod photoreceptor common precursors and mature rod photoreceptors (Koso et al., 2009), corroborating this sorting strategy. For the figure, images were created using FlowJo Software version 10.6.2 for Mac (BD).

RT-PCR. Total RNA of sorted photoreceptors and whole retinae were isolated with the RNeasy Micro and Mini Kit (Qiagen), respectively. RNA was reverse transcribed to cDNA using the iScript cDNA Synthesis Kit (BIO-RAD). To exclude amplification of genomic DNA, control experiments were performed in which reverse transcriptase was omitted. Possible contamination artifacts were excluded by replacing the template with water. Both controls were negative. Table 1 summarizes the primers used for amplification. The low-voltage-activated (LVA) primers have been successfully applied for the investigation of mouse islet cells (Vignali et al., 2006). For RT-PCR, degenerated primers which bind to every known LVA channel ($Ca_v3.1$, $Ca_v3.2$, $Ca_v3.3$) were used. Subsequently, specific primer pairs for each LVA Ca^{2+} channel were used for a nested PCR. For all PCRs, a standard PCR protocol with Taq DNA Polymerase (Qiagen) was used. Amplicon sizes were verified on 1.5% agarose gels stained with EtBr (Carl Roth). Images were arranged using CorelDRAW 2019 (Corel).

Electrophysiology and slice preparation. First, mice were sedated with isoflurane (3% inhalant) and killed by cervical dislocation. The preparation of horizontal retina slices has been described in detail in a previous article (Feigenspan and Babai, 2017). Eyes were enucleated, then the retina was removed from the eyeball and cut into six to eight pieces. Retina pieces were embedded into 1.8% low-melting agarose dissolved in Ames' Medium (Sigma-Aldrich). Horizontal slices, 160–180 µm thick, were cut with a vibratome (Leica Microsystems), and kept

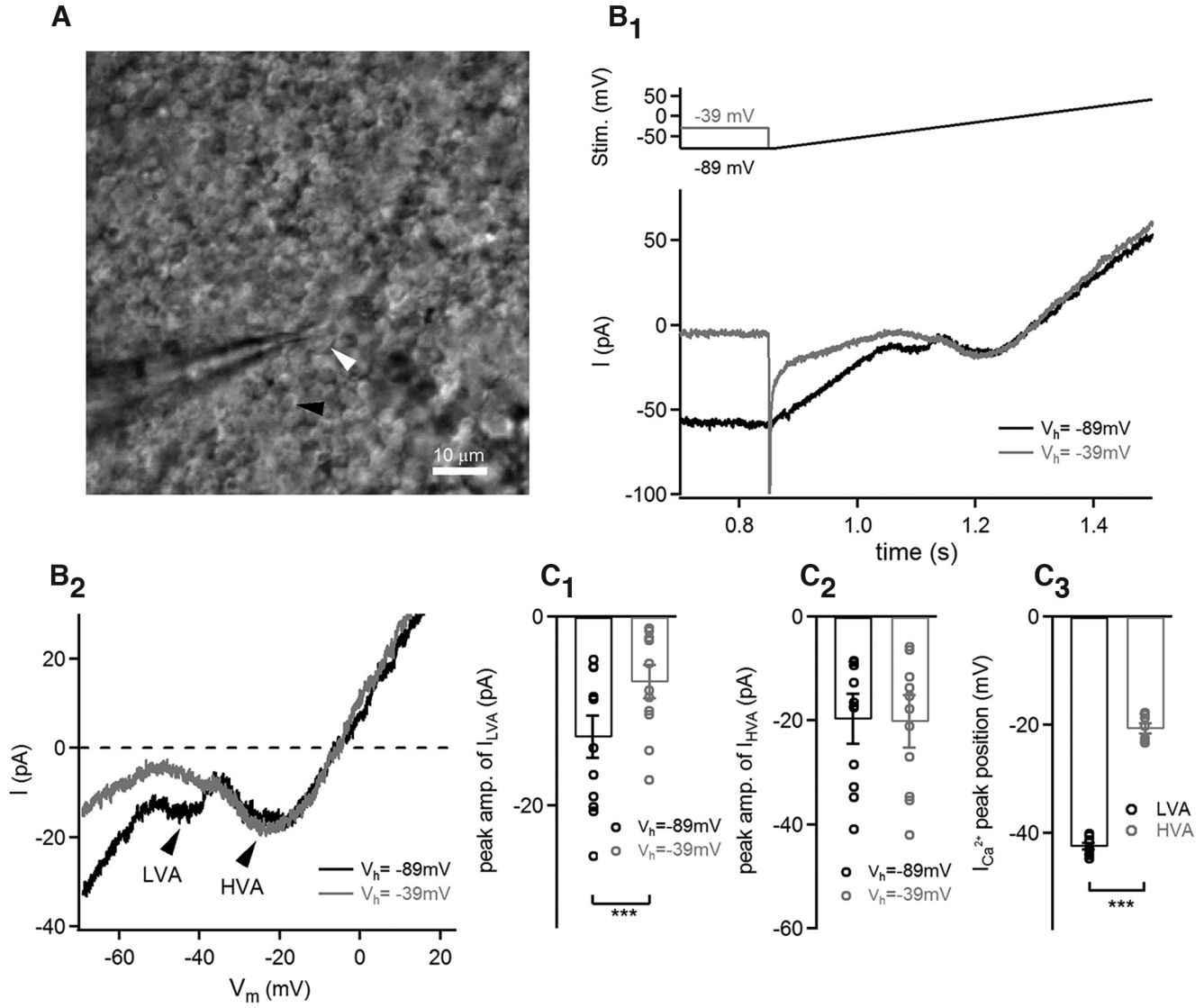

Figure 1. The presence of I_{LVA} and I_{HVA} in cone photoreceptors. ***A***, Example transmission microscope image of a patch-clamp recording from a cone photoreceptor terminal in a mouse horizontal retinal slice. White arrowhead, Cone photoreceptor terminal; black arrowhead, rod photoreceptor terminal. ***B_1***, Example whole-cell patch-clamp recording from mouse cone photoreceptor terminals. Currents were monitored in response to a voltage ramp protocol from −89 to +49 mV, with a speed of 0.1875 mV/ms. Prepulse duration was 800 ms at different V_h values (black, −89 mV; gray, −39 mV). ***B_2***, Example trace shows the current–voltage relationship of I_{Ca}. Arrowheads indicated I_{LVA} and I_{HVA} components. ***C_1–C_3***, Peak amplitudes of I_{LVA}: V_h = −89 mV: −12.72 ± 2.15 pA, $n = 12$; V_h = −39 mV: −6.90 ± 1.53 pA, $n = 12$; $p < 0.0001$, paired t test. Peak amplitudes of I_{HVA}: V_h = −89 mV: −19.66 ± 3.33 pA, $n = 12$; V_h = −39 mV: −20.19 ± 3.45 pA, $n = 12$; $p = 0.4511$, paired t test. I_{Ca} peak position: LVA: −42.48 ± 0.46 mV, $n = 12$; HVA: −20.75 ± 0.71 mV, $n = 12$; $p < 0.0001$, Mann–Whitney test.

in Ames' Medium at 37°C in an incubator containing 5% CO_2 and 55% O_2 for 20–30 min. For light-response experiments, mice were dark adapted for at least 1 h. Then, retinal slices and patch-clamp experiments were performed under dim red light (background illumination, 1 mW/m^2).

Retinal slices were observed with a 63× water-immersion objective (Zeiss) using a fixed-stage microscope (Axio Examiner, Zeiss) equipped with Dodt contrast. Whole-cell currents were recorded from cone photoreceptor terminals in a horizontal slice of the retina with an EPC-10 Patch-Clamp Amplifier (Heka Elektronik), low-pass filtered at 2.9 kHz using a built-in Bessel filter, and digitized at 10 kHz with Patchmaster software (Heka Elektronik). Voltages were corrected for liquid junction potentials (9 mV). Recordings were conducted at room temperature (22–24°C) and near body temperature (~33°C). Patch electrodes were pulled from borosilicate glass (Sutter Instrument) to a final resistance of 8–12 MΩ. Electrode tips were coated with Sylgard 184 (Dow Corning), and their series resistance (10–30 MΩ) was compensated up to 66%. Electrodes were positioned with NMN-21 micromanipulators (NARISHIGE Group). Retinae were superfused in every physiological experiment with 8 μM 6-cyano-7-nitroquinoxaline-2,3-dione (CNQX) to block the activation of postsynaptic AMPA and kainate receptors. We used the VM8 Perfusion System (ALA Scientific Instruments) for the local application of agonist and antagonist substances. The puffing solution, similar to the bath solution, always contained 8 μM CNQX. Preparations were continuously superfused at ~1 ml/min with extracellular solution containing the following (in mmol/L^{-1}): 116 NaCl, 22.6 $NaHCO_3$, 1.25 NaH_2PO_4, 2.5 KCl, 2 $CaCl_2$, 1 $MgCl_2$, 10 glucose, and 5 HEPES, at pH 7.4, bubbled with 95% O_2/5% CO_2. The intracellular solution contained the following (in mmol/L^{-1}): 136.6 Cs-gluconate, 5 EGTA, 13 tetraethylammonium chloride (TEA-Cl), 15 HEPES, 4 Mg-ATP, and 0.4 GTP, at pH 7.2. K-based intracellular solution contained the following (in mmol/L^{-1}): 134.5 K-gluconate, 10 KCl, 10 HEPES, 5 EGTA, 1 $CaCl_2$, 1 $MgCl_2$, 0.5 Na-GTP, and 4 Mg-ATP, at pH 7.2. All chemical reagents were obtained from Sigma-Aldrich except when specified otherwise.

Capacitance measurements were made using the Sine + DC technique, the lockin extension of the EPC-10 amplifier (sine wave frequency, 800 Hz; peak amplitude, 30 mV). We blanked output from the

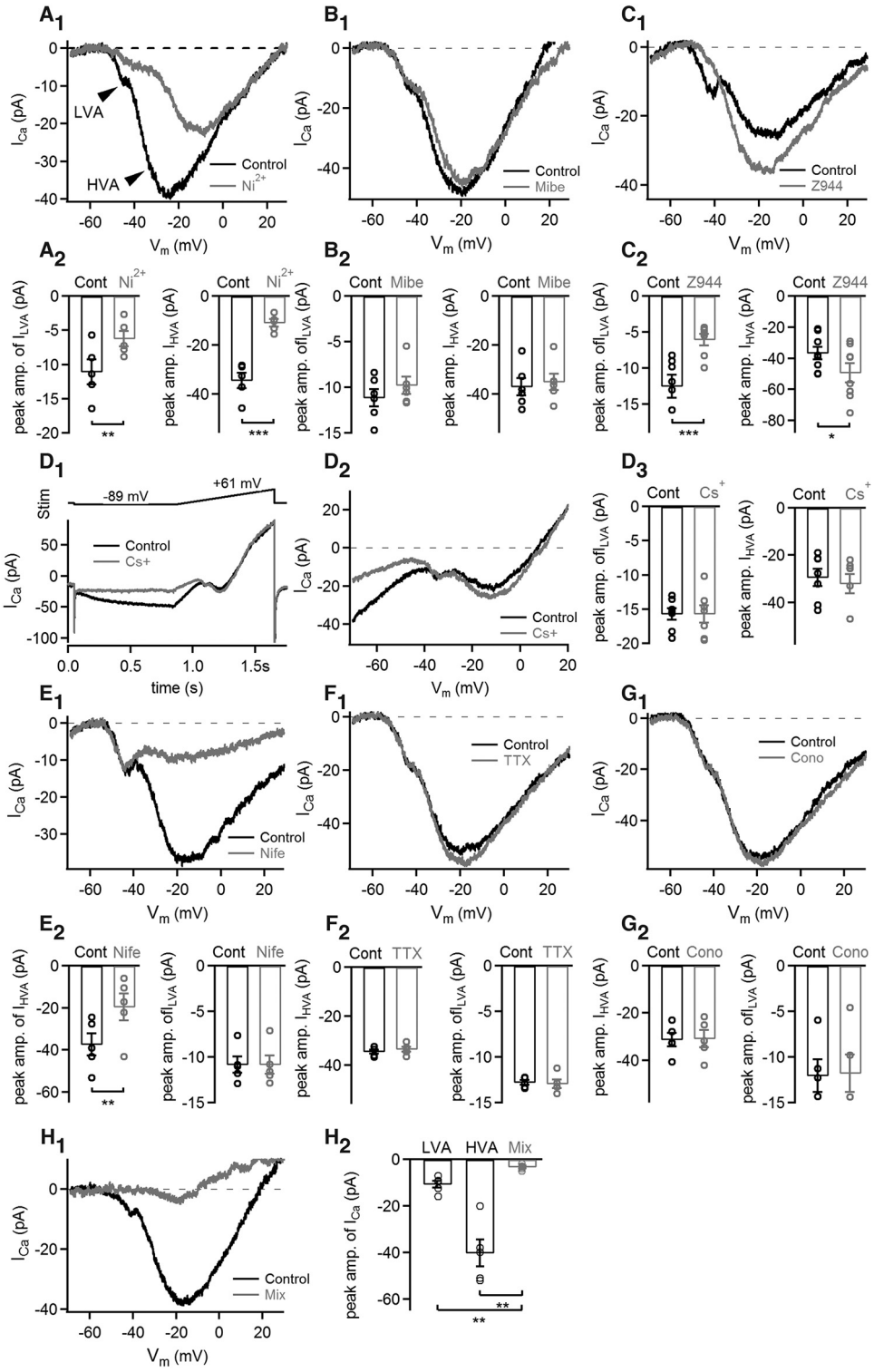

Figure 2. Pharmacological separation of I_{LVA} from I_{HVA}. ***A*$_1$**, Example current–voltage relationship of ramp-evoked I_{Ca} in mouse cone photoreceptors in the presence and absence of 100 μM $NiCl_2$. Arrowheads indicate I_{LVA} and I_{HVA} component (LVA, HVA). ***A*$_2$**, Peak I_{LVA} amplitude: control: −11.03 ± 1.80 pA, $n = 5$; nickel (Ni^{2+}): −6.22 ± 1.13 pA, $n = 5$; $p = 0.0030$, paired t test. Peak I_{HVA} amplitude: control: −37.45 ± 5.25 pA, $n = 5$; nickel (Ni^{2+}): −11.01 ± 1.52 pA, $n = 5$; $p = 0.0022$, paired t test. ***B*$_1$**, Example current–voltage relationship of evoked I_{Ca} in the presence and absence of 1 μM mibefradil (Mibe). ***B*$_2$**, Peak I_{LVA} amplitude: control: −11.15 ± 0.94 pA, $n = 6$; mibefradil: −9.81 ± 0.93 pA, $n = 6$; $p = 0.0641$, paired t test. Peak I_{HVA} amplitude: control: −37.04 ± 3.48 pA, $n = 6$; mibefradil: −35.06 ± 3.27 pA, $n = 6$; $p = 0.1712$, paired t test. ***C*$_1$**, Example current–voltage relationship of evoked I_{Ca} in the presence and absence of 5 μM Z944. ***C*$_2$**, Peak I_{LVA} amplitude: control: −12.51 ± 1.58 pA, $n = 7$; Z944: −6.05 ± 0.82 pA, $n = 7$; $p = 0.0003$, paired t test. Peak I_{HVA} amplitude: control: −36.61 ± 4.06 pA, $n = 7$; Z944: −49.25 ± 6.04 pA, $n = 7$; $p = 0.0371$, paired t test. ***D*$_1$**, Current response to a voltage ramp protocol from −89 to +61 mV, with a speed of 0.1875 mV/ms in the presence (gray) and absence (black) of 3 mM CsCl. Prepulse duration was 800 ms. ***D*$_2$**, Example trace shows current–voltage relationship of I_{Ca} during 3 mM CsCl application. ***D*$_3$**, Peak I_{LVA} amplitude: control: −15.72 ± 0.87 pA, $n = 7$; CsCl: −15.71 ± 1.25 pA, $n = 7$; $p = 0.9786$, paired t test. Peak I_{HVA} amplitude: control: −29.42 ± 3.71 pA, $n = 7$; CsCl: −32.09 ± 4.05 pA, $n = 7$; $p = 0.0933$, paired t test. ***E*$_1$**, Example current–voltage relationship of evoked I_{Ca} in the presence and absence of 10 μM nifedipine (Nife). ***E*$_2$**, Peak I_{HVA} amplitude: control: −37.45 ± 5.25 pA, $n = 5$; nifedipine: −19.73 ± 6.42 pA, $n = 5$; $p = 0.0022$, paired t test. Peak I_{LVA} amplitude: control: −10.83 ± 0.87 pA, $n = 5$; nifedipine: −10.86 ± 1.00 pA, $n = 5$; $p = 0.9082$, paired t test. ***F*$_1$**, Example

phase-lock amplifier for 10 ms after the step and began measurements 10 ms later to circumvent any influence of gating charges and let time for the phase angle feedback circuitry to settle. Recordings were only evaluated if access resistance was <38 MΩ and holding current was under −30 pA at holding potential (V_h) = −60 mV. Average resting membrane capacitance (C_m), membrane resistance, and access resistance values for cone photoreceptors were 3.53 ± 0.18 pF, 1148.16 ± 125.80 MΩ, and 32.47 ± 2.76 MΩ, respectively. Full-field light stimulation (~130 W/cm^2 irradiance) was generated by a xenon arc lamp of the lambda DG4 illumination system (Sutter Instrument). Light signals were conveyed to the sample via fiber optics.

To distinguish cone from rod photoreceptors we performed whole-cell recordings and compared the resting C_m and I_{Ca} amplitude of the two photoreceptor types. We found no overlap in the distribution of C_m and I_{Ca} (C_{m_rod}, 1.32 ± 0.21 pF; C_{m_cone}, 3.53 ± 0.18 pF; I_{Ca_rod}, −8.78 ± 0.43 pA; I_{Ca_cone}, −36.04 ± 2.31 pA; n = 10 and 26, respectively). Additionally, we compared HVA and LVA I_{Ca} values recorded from fluorescently labeled cone photoreceptor terminals of Rac3-eGFP mice and from cone photoreceptor terminals of C57BL/6 mice. We found nonsignificant differences [LVA current $(I_{LVA})_{Rac}$: −11.37 ± 0.86 pA; I_{LVA_WT}: −11.40 ± 0.80 pA; p = 0.9846; HVA current $(I_{HVA})_{Rac}$: −35.52 ± 1.55 pA; I_{HVA_WT}: −36.04 ± 2.31 pA; p = 0.8681; n = 9 and 13, respectively, unpaired t test]. These experiments strongly indicate that the identification of cone photoreceptors in our experiments was successful.

Statistical analysis. Statistical analysis and data visualization were done using GraphPad Prism (GraphPad Software) and Igor Pro 6.3 (WaveMetrics, Inc.). Data are reported as the mean ± SEM, and n indicates the number of cells measured. For each experiment, at least three mice were used. If the statement of normality was met by the Kolmogorov–Smirnov test ($p > 0.05$) to data points, mean values were compared using a paired two-sample t test. The Mann–Whitney U test was used when the normal distribution assumption was not encountered. For clearness of illustration, current traces were low-pass filtered at 1 kHz. In all figures, significance was identified as follows: $^*p < 0.05$, $^{**}p < 0.01$, and $^{***}p < 0.001$.

Results

Mouse cone photoreceptors exhibit I_{LVA} and I_{HVA}

First, we examined the voltage dependence of I_{Ca} in mouse cone photoreceptors. We prepared horizontal slices of the retina (Feigenspan and Babai, 2017) in which a horizontal cut was made through the outer plexiform layer to reveal cone photoreceptor terminals (Fig. 1*A*, white arrowhead). Cone photoreceptor terminals were discriminated from rod photoreceptor terminals (Fig. 1*A*, black arrowhead) by their size, anatomic localization, and I_{Ca} amplitude (see Materials and Methods). Cone photoreceptor terminals are approximately threefold bigger and localize closer to the inner retina than the relatively small rod photoreceptor terminals. Additionally, cone photoreceptors display I_{Ca} amplitudes that are six to eight times bigger than that of rod photoreceptors. To isolate I_{Ca}, we used a cesium and TEA-Cl-based intracellular solution with 2 mM $CaCl_2$ in the bath solution as the charge carrier. To exclude feedback from horizontal cells, the extracellular solution contained 8 µM CNQX, which is a potent AMPA and kainate receptor antagonist (Feigenspan and Babai, 2015; Babai et al., 2016). For the recording, we used pipettes with ~10 MΩ resistance pulled from borosilicate glass (Sutter Instrument), and we achieved a final access resistance of 20–30 MΩ. Series resistance was compensated up to 66%. We rejected recordings with a larger than −30 pA leak current at −69 mV V_h. Cone photoreceptors were held at −69 mV, and I_{Ca} was measured by using a ramp voltage protocol from −89 mV (800 ms) to +49 mV with a speed of 0.1875 mV/ms (Fig. 1*B1*, *B2*). Surprisingly, the I_{Ca} trajectory showed two peaks, one at a lower (Fig. 1*B2*, LVA) and one at a higher (Fig. 1*B2*, HVA) membrane potential (V_m) range. The double peak seen in the current–voltage profile of cone photoreceptor I_{Ca} is comparable to I_{Ca} in certain types of retinal bipolar and horizontal cells where both HVA (L-type) and LVA (T-type) Ca^{2+} channels are present (Hu et al., 2009; Feigenspan et al., 2020). Therefore, we next measured I_{Ca} using the same voltage ramp protocol but starting from a more depolarized V_h value of −39 mV (800 ms). At this slightly depolarized V_m, LVA T-type Ca^{2+} channels typically show strong inactivation (Perez-Reyes, 2003), while HVA L-type Ca^{2+} channels only inactivate moderately (Taylor and Morgans, 1998). Consequently, only I_{HVA} should appear in the current trajectory. As a result, we found that the amplitude of I_{LVA} significantly decreased, but that of I_{HVA} did not change (Fig. 1*B2*,*C1*,*C2*). The peak of I_{LVA} and I_{HVA} localized at approximately −40 mV and approximately −20 mV, respectively (Fig. 1*C3*), and the presence of the two current types yielded a wide range of responsive V_m. The first peak suggested the presence of T-type Ca^{2+} channels because the typical T-type I_{Ca} reaches its maximal amplitude between −40 and −10 mV (Ertel et al., 1997). However, unlike T-type I_{Ca} in other tissues, I_{LVA} was not fully inactivated at −39 mV, a potential that is close to the physiological V_m in darkness (−40 mV). In summary, patch-clamp recordings from the terminal of cone photoreceptors indicate the unexpected presence of an I_{LVA}, suggesting the expression of T-type Ca^{2+} channels in cone photoreceptors additionally to L-type Ca^{2+} channels.

Pharmacological isolation of LVA and HVA I_{ca}

The pore-forming subunits of the T-type Ca^{2+} channel family consist of three members: $Ca_v3.1$ (α1G), $Ca_v3.2$ (α1H), and $Ca_v3.3$ (α1I), which show similar activation and inactivation kinetics (Klöckner et al., 1999; Perez-Reyes, 2003). Nickel blocks all three T-type Ca^{2+} channel members at higher concentrations, but it selectively blocks $Ca_v3.2$ channels at lower concentrations (Lee et al., 1999, 2002; Kang et al., 2006). We applied 100 µM nickel and stimulated cone photoreceptors with a ramp voltage protocol described in Figure 1. Example I_{Ca} responses are illustrated in Figure 2*A1*. We used a pressure-controlled puffing system (model ALA-VM8, ALA Scientific Instruments), which allowed the fast and local application of nickel and CNQX (8 µM) containing solution through a 75-µm-diameter tube directly onto cone photoreceptor terminals. Control I_{Ca} was measured during the puff application of the bath solution to exclude changes caused by mechanical effects. We found that the application of nickel caused a ~70% and a ~50% reduction of I_{HVA} and I_{LVA} components, respectively (Fig. 2*A1*,*A2*). Nickel is a commonly described ion that blocks LVA Ca^{2+} channels, but HVA Ca^{2+} channels, especially L-type Ca^{2+} channels, also show nickel sensitivity (Zamponi et al., 1996; Bradley et al., 2004; To et al., 2020). Therefore, the reduction of the I_{HVA} component is

←

current–voltage relationship of evoked I_{Ca} in the presence and absence of 1 µM TTX. ***F*$_2$**, Peak I_{LVA} amplitude: control: −12.80 ± 0.26 pA, n = 5; TTX: −12.92 ± 0.47 pA, n = 5; p = 0.7628, paired t test. Peak I_{HVA} amplitude: control: −34.51 ± 0.81 pA, n = 5; TTX: −33.61 ± 1.02 pA, n = 5; p = 0.2789, paired t test. ***G*$_1$**, Example current–voltage relationship of evoked I_{Ca} in the presence and absence of 10 µM ω-conotoxin GVIA (Cono). ***G*$_2$**, Peak I_{LVA} amplitude: control: −12.05 ± 1.77 pA, n = 5; Cono: −11.81 ± 2.06 pA, n = 5; p = 0.7978, paired t test. Peak I_{HVA} amplitude: control: −31.37 ± 2.92 pA, n = 5; Cono: −31.03 ± 3.60 pA, n = 5, p = 0.7205; paired t test. ***H*$_1$**, Example current–voltage relationship of evoked I_{Ca} in the presence and absence of (3 mM CsCl, 10 µM nifedipine, 5 µM Z944 and 100 µM nickel). ***H*$_2$**, Peak I_{LVA} amplitude (LVA), −10.72 ± 1.53 pA; peak I_{HVA} amplitude (HVA), −40.16 ± 5.78 pA; peak I_{Ca} amplitude in the presence of L-type and T-type Ca^{2+} channel blockers (Mix), −3.0 ± 0.33 pA. LVA versus mix, p = 0.005; HVA versus mix, p = 0.0028; n =5, unpaired t test.

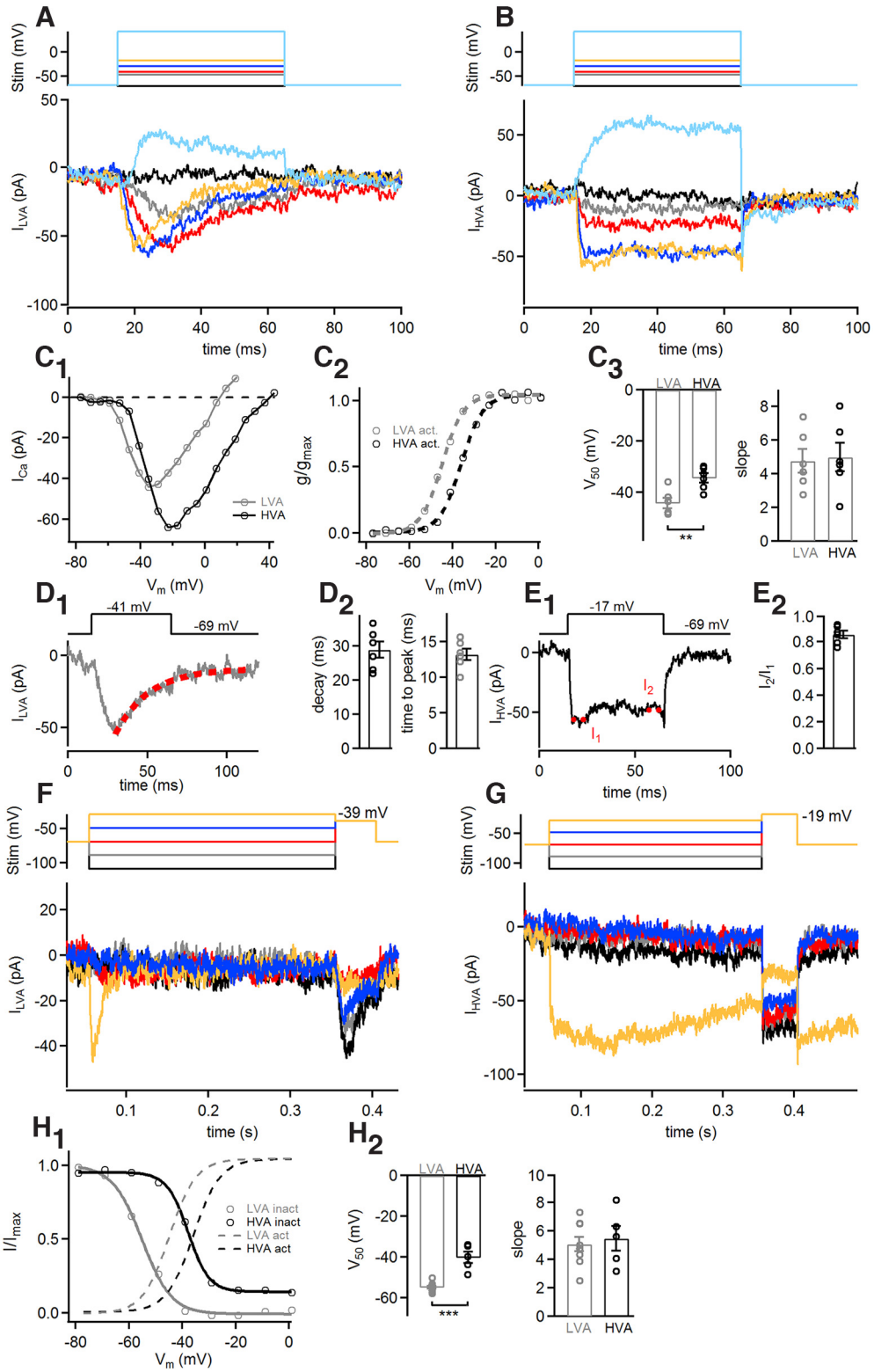

Figure 3. Physiological properties of I_{LVA} and I_{HVA}. ***A***, Representative examples of I_{LVA} in cone photoreceptors evoked by 50 ms voltage steps to different potentials (V_h = −62, −38, −32, −20, −8, and 52 mV) in the presence of 8 μM CNQX, 3 mM CsCl, and 10 μM nifedipine. ***B***, Representative examples of I_{HVA} evoked by 50 ms voltage steps to different potentials (V_h = −62, −38, −32, −20, −8, and 52 mV) in the presence of 8 μM CNQX, 3 mM CsCl, and 5 μM Z944. ***C_1***, Current–voltage relationship of I_{LVA} and I_{HVA} currents evoked by voltage steps from −77 to 43 mV by 6 mV steps. ***C_2***, Voltage dependence of steady-state activation of I_{LVA} and I_{HVA} (g/g_{max}). Data points were fitted with the Boltzmann function (dashed lines). ***C_3***, Mean V_{50}: I_{LVA}, −44.17 ± 1.98 mV; I_{HVA}, −34.38 ± 1.78 mV; n = 6; p = 0.0043, unpaired t test. Mean activation slope factor (slope): I_{LVA}, −4.77 ± 0.70; I_{HVA}, 4.99 ± 0.83; n = 6; p = 0.8417, unpaired t test. ***D_1***, Typical maximal I_{LVA} in cone photoreceptors evoked by a voltage step from −69 to 41 mV (50 ms). The dashed red line indicates I_{LVA} decay fitted with an exponential function. ***D_2***, Corresponding time to I_{LVA} peak, 13.18 ± 0.81 ms. Decay, tau of single exponential function: 28.82 ± 2.38 ms. ***E_1***, Typical maximal I_{HVA} in cone photoreceptors evoked by a voltage step from −69 to −17 mV (50 ms). ***E_2***, Corresponding fast inactivation ratio, 0.85 ± 0.03. ***F***, Example traces showing the steady-state inactivation of I_{LVA}. A 300-ms-long conditioning pulse over a series of V_h, from −100 to −20 mV (20 mV increments), was applied before the test pulse (−39 mV, 50 ms). ***G***, Example traces showing the steady-state inactivation of I_{HVA}. The 300-ms-long conditioning pulse over a series of V_h values from −100 to −20 mV (20 mV increments) was applied before the test pulse (−19 mV, 50 ms). ***H_1***, Steady-state inactivation of I_{LVA} and I_{HVA} were

unsurprising. To further analyze the origin of the I_{LVA} component, we puffed 1 μM mibefradil, a T-type Ca^{2+} channel blocker (Martin et al., 2000), onto cone photoreceptor terminals. However, we only found a slight tendency for reduced amplitudes for both I_{LVA} and I_{HVA} (Fig. 2*B1*,*B2*). We did not use a higher concentration of mibefradil to isolate T-type Ca^{2+} channels because it has been shown that mibefradil is also an antagonist for L-type Ca^{2+} channels (Leuranguer et al., 2001; Lee et al., 2006; To et al., 2020), and Cl^-, K^+, and Na^+ channels (Heady et al., 2001). Next, we tested 5 μM Z944, a selective T-type Ca^{2+} channel antagonist (Casillas-Espinosa et al., 2015), which significantly decreased I_{LVA} amplitude but unexpectedly increased the I_{HVA} component (Fig. 2*C1*,*C2*), revealing Z944 as a possible agonist for L-type Ca^{2+} channels in cone photoreceptors. In general, the sensitivity of I_{LVA} to nickel and Z944 suggests the presence of T-type Ca^{2+} channels in cone photoreceptors, and the sensitivity of I_{HVA} to Z944 suggests that the L-type Ca^{2+} channel in cone photoreceptors may have unique molecular properties.

Next, we confirmed whether other non-T-type Ca^{2+} channels contribute to I_{LVA}. We tested whether the hyperpolarization-activated cation current (I_h), which is responsible for shaping the photoreceptor light response (Akopian and Witkovsky, 1996), affects Ca^{2+} currents by puff application of 3 mM CsCl (Fig. 2*D1*, *D2*). We found no significant change in I_{LVA} and I_{HVA} amplitudes (Fig. 2*D3*), suggesting that the measured I_{LVA} was because of T-type Ca^{2+} channels and not hyperpolarization-activated cation channels. To inhibit the I_{HVA} component, we used 10 μM nifedipine, an L-type Ca^{2+} channel blocker. Nifedipine has a high affinity to L-type and a very low affinity to T-type Ca^{2+} channels (Stengel et al., 1998). Nifedipine significantly blocked the I_{HVA} component, but left the I_{LVA} component untouched (Fig. 2*E1*,*E2*). This indicates that the I_{LVA} component was not because of the activation of HVA L-type Ca^{2+} channels, further providing evidence for the presence of LVA T-type Ca^{2+} channels in mouse cone photoreceptors. Finally, we verified whether tetrodotoxin (TTX)-sensitive Na^+ channels or ω-conotoxin GVIA-sensitive N-type Ca^{2+} channels influenced I_{LVA} or I_{HVA}. During puff application of 1 μM TTX (Fig. 2*F1*,*F2*) or 1 μM ω-conotoxin GVIA (Fig. 2*G1*,*G2*), we found no significant difference in I_{HVA} and I_{LVA} Ca^{2+} current amplitudes (Fig. 2*F2*,*G2*). Measuring I_{Ca} in the presence of a mixture of antagonistic compounds, including T-type and L-type Ca^{2+} channel blockers (10 μM nifedipine, 5 μM Z944, and 100 μM nickel additionally to 8 μM CNQX and 3 mM CsCl), resulted in a rather small residual current (Fig. 2*H1*,*H2*), which indicates a minimal nonspecific effect. In conclusion, the results from our pharmacological experiments strongly indicate the presence of T-type Ca^{2+} channels in addition to L-type Ca^{2+} channels in mouse cone photoreceptors.

Biophysiological characterization of I_{LVA} and I_{HVA}

In the next set of experiments, we measured the electrophysiological properties of I_{LVA} and I_{HVA} components. I_{LVA} was isolated by puff application of 8 μM CNQX, 3 mM CsCl, and 10 μM nifedipine containing extracellular solution, thereby removing any postsynaptic feedback, I_h, and I_{HVA} components. In this condition, I_{LVA} of cone photoreceptors was recorded in response to a series of voltage step stimulations (50 ms) from $V_h = -69$ mV (Fig. 3*A*). Furthermore, based on the results of our pharmacological experiments (Fig. 2), we chose 8 μM CNQX, 3 mM CsCl, and 5 μM Z944 to isolate I_{HVA}. In this condition, I_{HVA} produced typical high-voltage-activated current trajectories in response to a series of voltage steps (Fig. 3*B*). The average I_{HVA} and I_{LVA} amplitude relationships to V_m (*I–V*) in cone photoreceptors are illustrated in Figure 3*C1*. Relative conductance values of I_{HVA} and I_{LVA} were fitted with a Boltzmann function to estimate the voltage dependency of the activation (Fig. 3*C2*). As expected, the half-activation (V_{50}) of I_{HVA} shifted to the right by ~10 mV compared with V_{50} of I_{LVA}, but slope values were comparable to each other (Fig. 3*C3*). Additionally, the time course of activation and inactivation of I_{LVA} was measured on maximal current amplitude traces, which were chosen from the step series. Maximal I_{LVA} amplitudes were typically evoked by a voltage step from −69 to −41 mV (50 ms; Fig. 3*D1*). Fast inactivation was estimated by fitting the decay phase of the current with an exponential function (Fig. 3*D1*) and found to be <30 ms (Fig. 3*D2*). Time to I_{LVA} peak values stayed at ~13 ms (Fig. 3*D2*). In general, the time courses of activation and inactivation kinetics of cone photoreceptor I_{LVA} were very similar to currents produced by other neuronal T-type Ca^{2+} channels (Klöckner et al., 1999). The time course of I_{HVA} inactivation was measured as the ratio of I_{HVA} amplitude at the beginning and the end of the current trace (Fig. 3*E1*). I_{HVA} showed an ~15% reduction during a voltage step to −17 mV (50 ms) from $V_h = -69$ mV (Fig. 3*E2*). HVA L-type Ca^{2+} currents typically show little fast inactivation in photoreceptors (Barnes and Hille, 1989; Yagi and Macleish, 1994). To determine the steady-state inactivation properties of I_{LVA} and I_{HVA} in cone photoreceptors, currents were elicited by test pulses either to −39 mV (I_{LVA}) or −19 mV (I_{HVA}) preceded by a series of conditioning potential steps ranging from −100 to 0 mV (duration, 300 ms; Fig. 3*F*,*G*). The inactivation was calculated by dividing the test pulse-evoked current amplitudes with maximal current amplitudes (I/I_{max}; Fig. 3*H1*). Data points were fitted by a Boltzmann function. Results indicated that V_{50} parameters of I_{HVA} inactivation were shifted to the right by ~15 mV, while slope values stayed similar (Fig. 3*H2*). Interestingly, the activation and inactivation curves of both I_{LVA} and I_{HVA} revealed a noninactivating current window in the range of the physiological V_m (−60 to −30 mV) where channel inactivation is incomplete and thus regulates steady-state Ca^{2+} levels (Fig. 3*H1*).

Ca^{2+} spikes are present in cone photoreceptors

LVA T-type Ca^{2+} channels are suggested to play a crucial role in the activity of several types of neurons in the CNS by generating low-threshold spikes and activating higher-threshold ion channels, which induce a burst of firing and oscillatory behavior (Perez-Reyes et al., 1998; Perez-Reyes, 2003). To investigate the impact of T-type Ca^{2+} channels on cone photoreceptor V_m changes, we performed whole-cell current-clamp recordings. Because the Cs^+-based and TEA-Cl-based pipette solution used in the previous experiments blocks K^+ currents, thereby increasing the input resistance of the cells and the probability of spiking,

←

calculated by normalizing the test pulse-evoked current amplitude to the maximum current amplitude and were plotted over the prepulse V_m. Data points were fitted with Boltzmann function and illustrated as solid black (I_{HVA}) and gray (I_{LVA}) lines. Dashed lines are the Boltzmann fits of the I_{LVA} and I_{HVA} activation kinetics from C_2. ***H2***, Mean V_{50}: I_{LVA}, −54.82 ± 0.81 mV; I_{HVA}, −40.11 ± 2.76 mV; $n = 8$ and $n = 5$; $p < 0.0001$, unpaired *t* test. Mean inactivation slope factor (slope): I_{LVA}, 5.06 ± 0.49; I_{HVA}, 5.45 ± 0.87; $n = 8$ and $n = 5$; $p = 0.6773$, unpaired *t* test.

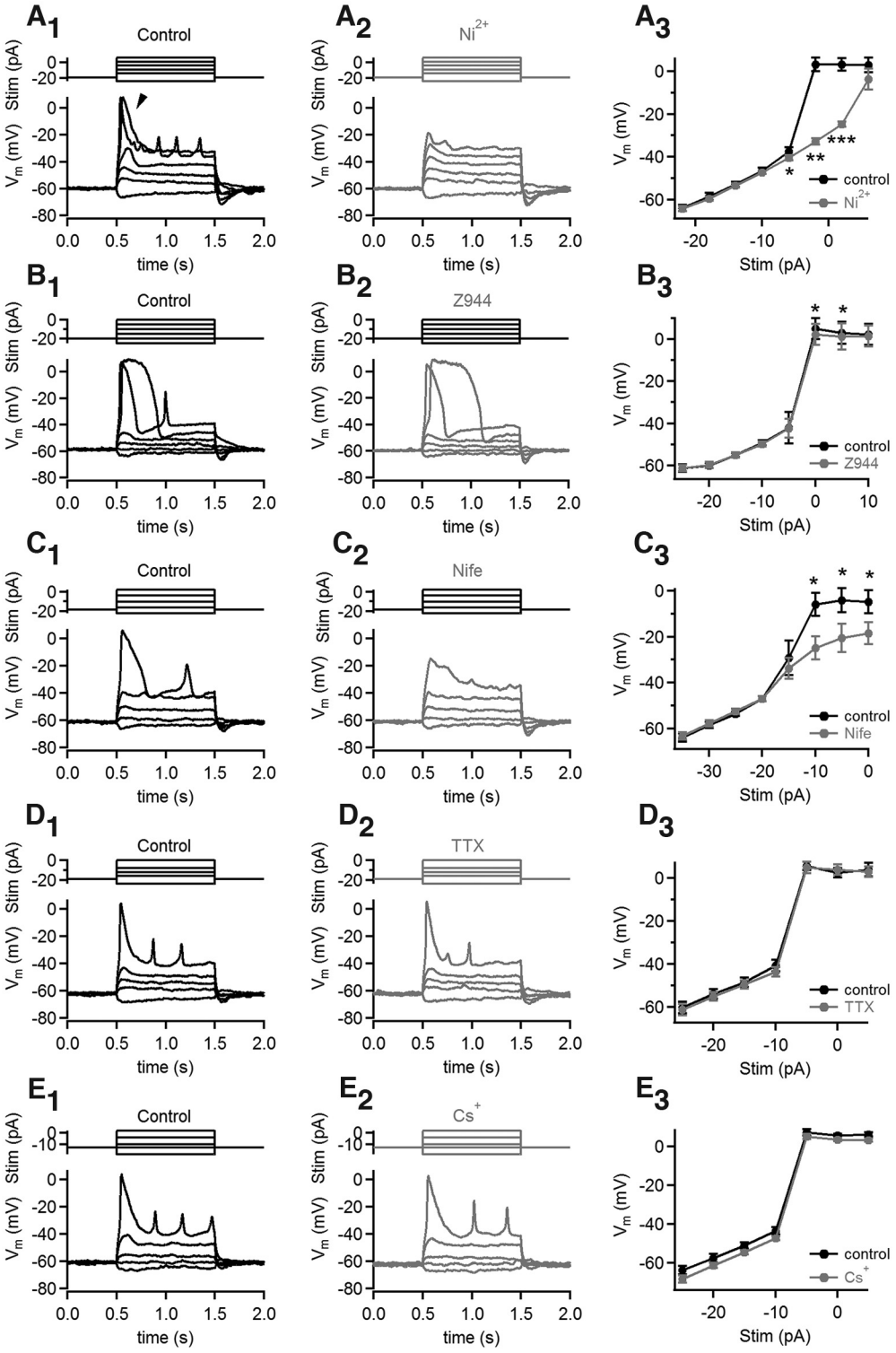

Figure 4. Ca^{2+} spikes present at cone photoreceptors. ***A1***, Example of cone photoreceptor V_m change to current injections (6, 1, −4, −9, −14, and −24 pA) in current-clamp mode using K^+-gluconate-based intracellular pipette solution. Arrowhead labels the initial fast rise of the V_m (spike) at the beginning of the stimulus. ***A2***, Example trace of cone photoreceptor V_m change to the same level of current injections in the presence of 100 μM nickel (Ni^{2+}). ***A3***, V_m amplitude versus stimulus intensity plot. Significance was tested with a paired *t* test among each stimulus intensity (−22 pA, $p = 0.7346$; −18 pA, $p = 0.1548$; −14 pA, $p = 0.2918$; −10 pA, $p = 0.3324$; −6 pA, $p = 0.0389$; −2 pA, $p < 0.0001$; 2 pA, $p < 0.0001$; 6 pA, $p = 0.2151$; $n = 6$). ***B1***, ***B2***, Example traces of cone photoreceptor V_m change to current pulses (0, −5, −10, −15, −20, and −25 pA), in the absence (control, ***B1***) and presence (gray, ***B2***) of 5 μM Z944. ***B3***, V_m amplitude versus stimulus intensity plot. Significance was tested with a paired *t* test in each stimulus intensity (−25 pA, $p = 0.9846$; −20 pA, $p = 0.9583$; −15 pA, $p = 0.9467$; −10 pA, $p = 0.1408$; −5 pA, $p = 0.3731$; 0 pA, $p = 0.0485$; 5 pA, $p = 0.0498$; 10 pA, $p = 0.2916$; $n = 7$). ***C1***, ***C2***, Example traces of cone photoreceptor V_m change to current pulses (2, −4, −10, −16, and −22 pA), in the absence (control; ***C1***) and presence (Nife; gray; ***C2***) of 10 μM nifedipine. ***C3***, V_m amplitude versus stimulus intensity plot. Significance was tested with a paired *t* test in each stimulus intensity (−35 pA, $p = 0.1143$; −30 pA, $p = 0.1352$; −25 pA, $p = 0.1362$; −20 pA, $p = 0.9151$; −15 pA, $p = 0.5775$; −10 pA, $p = 0.0150$; −5 pA, $p = 0.0199$; 0 pA, $p = 0.050$; $n = 6$). ***D1***, ***D2***, Example traces of cone photoreceptor V_m change to current pulses (0, −8, −12, −16, and −24 pA), in the absence (control; ***D1***) and presence (TTX; gray; ***D2***) of 1 μM tetrodotoxin. ***D3***, V_m amplitude versus stimulus intensity plot. Significance was tested with paired *t* test in each stimulus intensity (−25 pA, $p = 0.296$; −20 pA, $p = 0.1322$; −15 pA, $p = 0.2485$;

we examined whether cone photoreceptors generate spikes in the presence of a K^+-gluconate-based intracellular solution. In the current-clamp configuration, we first injected steady currents to keep V_m hyperpolarized (approximately −60 mV) and then depolarized cone photoreceptors stepwise by steady current injection to mimic different levels of light exposure. Figure 4*A1* shows an example of the V_m changes of a cone photoreceptor in response to a current injection series from −24 to +6 pA (Δ5 pA, 1 s). When cone photoreceptor V_m was held at a hyperpolarized level of approximately −60, and approximately −50 mV by steady current injection, we did not observe any spike behavior. When V_m reached a threshold of approximately −40 mV, V_m showed a fast rise, which generated an immediate large spike (arrowhead) and additional smaller spikes with some delay (Fig. 4*A1*). The amplitude of a spike is classically dependent on how long the responsible ion channels are open at the rising phase. Therefore, for the higher spike peaks L-type Ca^{2+} channels could be responsible as they do not inactivate strongly (Fig. 3*E*). To determine the ion channel involvement in the observed spikes, we performed puff application of several pharmacological agents during the current injections described above. We could not evoke spikes during the puff application of 100 µM nickel onto the cone photoreceptor terminal (Fig. 4*A2*). In this condition, the V_m at the beginning of the stimuli stayed well below that seen in control conditions, and the injected current–V_m plot stayed rather linear in the range of physiological V_m (Fig. 4*A3*). We also tested the effect of Z944 on cone photoreceptor spike generation. The 5 µM Z944 blocked I_{LVA} but increased I_{HVA} in the previous experiment (Fig. 2*C1*,*C2*). Here, spikes could still be generated by current injections; however, peak V_m stayed slightly, but significantly, below control values (Fig. 4*B1–B3*). This suggests that an increased level of HVA L-type Ca^{2+} current could partially compensate for the reduced level of LVA T-type Ca^{2+} current considering spike generation. This assumption is also supported by the results of the next experiment, where the application of the L-type Ca^{2+} channel blocker nifedipine (10 µM) blunted the initial V_m rise (Fig. 4*C1*,*C2*). However, peak V_m values (Fig. 4C_3, gray trace) were less linear than what was observed in the presence of nickel (Fig. 4*A3*, gray trace). The slight depolarization remaining in the presence of nifedipine at more than −40 mV V_m suggests that the activation of T-type Ca^{2+} channels helps to boost the rising phase of the depolarization to then activate L-type Ca^{2+} channels. Next, we tested for the possible role of Na^+ channels in spike generation. During puff application of 1 µM TTX, the depolarization evoked by a series of current injections was not altered (Fig. 4*D1–D3*). Additionally, by puffing 3 mM CsCl, we also found that I_h did not significantly influence cone photoreceptor spiking behavior (Fig. 4*E1–E3*). Altogether, the experiments indicate that the spiking behavior in cone photoreceptors at depolarized V_m is because of the cooperative activation of both T-type and L-type Ca^{2+} channels.

Self-generating spike behavior at depolarized V_m

In the next set of experiments, we asked whether cone photoreceptors generate spikes spontaneously at dark V_m. Therefore, we injected a steady current for 10 s in the current-clamp configuration to keep the V_m of cone photoreceptors close to −40 mV, a typical dark V_m. As in the previous experiment, we used K^+-gluconate-based intracellular pipette solution to keep input resistance more physiological. Remarkably, in this condition, cone photoreceptors repeatedly generated spikes. Figure 5*A1* shows a representative example of cone photoreceptor spiking behavior when cone photoreceptor V_m was adjusted to approximately −40 mV by injecting −3 pA current. Puff application of 100 µM nickel onto the cone photoreceptor terminal blocked spikes completely in seven of seven cells (Fig. 5*A2*), and the effect could be washed out after a few minutes. The application of 10 µM nifedipine similarly blocked spike activity in six of six cells (Fig. 5*B2*), and the effect could be washed out after several minutes. Additionally, we tested the effect of 5 µM Z944 on spontaneous spike generation in cone photoreceptors. In this condition, spikes could still be observed with a frequency similar to control conditions (Fig. 5*C1–C3*), but the peak amplitude and the half-width of the spikes were significantly altered (Fig. 5*C3*). These results fit well with the examined effect of Z944 on I_{LVA} and I_{HVA} (Fig. 2). In summary, the effect of Z944 on spike kinetics and amplitude and the elimination of spontaneous spikes by nickel and nifedipine indicate that both L-type and T-type Ca^{2+} channels are responsible for the spontaneous spike generation in cone photoreceptors. Because spikes are typically associated with Na^+ channels, we also examined whether 1 µM TTX inhibits spike generation. We found no significant difference in spike frequency ($p = 0.4712$, $n = 4$) and peak amplitude ($p = 0.3820$, $n = 4$) compared with control conditions. Examination of spontaneous spike behavior in the presence of 3 mM CsCl also showed no significant changes in spike frequency and peak amplitude ($p = 0.2641$, $p = 0.2131$, respectively, $n = 4$), suggesting no role of I_h in spike generation. In $I = 0$ recording mode, cone photoreceptors showed an average V_m of −37.01 ± −4.23 mV (n =11). At this potential, cone photoreceptors also consistently generated spontaneous spikes. In general, the analysis of control spikes indicated an average frequency of ∼1.5 Hz, a peak amplitude of approximately −13.5 mV, a baseline of approximately −40.5 mV, and a half-width of ∼32 ms (Fig. 5*D*). These parameters are different from Na^+ action potential parameters measured in a typical mammalian central neuron (Bean, 2007). To further analyze the kinetics of the spontaneous spike events in cone photoreceptors, we picked representative, individual spikes from the recordings at depolarized V_m (approximately −40 mV), as illustrated in Figure 5*E1*. Initially, we created trajectory plots of spike rate of change (Fig. 5*E2*), and we measured the rise rate of V_m. We determined the spike threshold as 7.5% of the maximal rise rate at 0.22 mV/ms (Fig. 5*E3*, gray horizontal line). This value yielded an average of −36.2 ± 1.05 mV (Fig. 5*E4*) for the activation threshold of spontaneous spikes (gray horizontal line), which is very close to the typical dark V_m (Ingram et al., 2020). We found a maximal rise rate of ∼3.1 mV/ms (Fig. 5*E4*). This value is 50–150 times slower than was measured for Na^+ action potentials (Hodgkin and Huxley, 1952), further strengthening the finding that spikes in cone photoreceptors are not generated by Na^+ channels. Altogether, these experiments showed that mouse cone photoreceptors are able to develop self-generating spike activity around the dark V_m. A plausible explanation for this oscillatory behavior in spike generation is the periodic activation and inactivation of LVA T-type Ca^{2+} channels, which further activate L-type Ca^{2+} channels (Perez-Reyes, 2003).

Another important question is whether these Ca^{2+} spikes have physiological relevance. Therefore, we investigated spontaneous

←

−10 pA, $p = 0.1641$; −5 pA, $p = 0.6813$; 0 pA, $p = 0.1703$; 5 pA, $p = 0.3681$; $n = 4$). ***E1***, ***E2***, Example traces of cone photoreceptor V_m change to current pulses (2, −4, −10, −13, and −19 pA), in the absence (control; ***E1***) and presence (Cs^+; gray; ***E2***) of 1 µM CsCl. ***E3***, V_m amplitude versus stimulus intensity plot. Significance was tested with paired t test in each stimulus intensity (−25 pA, $p = 0.2575$; −20 pA, $p = 0.2498$; −15 pA, $p = 0.2172$; −10 pA, $p = 0.1939$; −5 pA, $p = 0.1366$; 0 pA, $p = 0.0712$; 5 pA, $p = 0.0512$; $n = 5$).

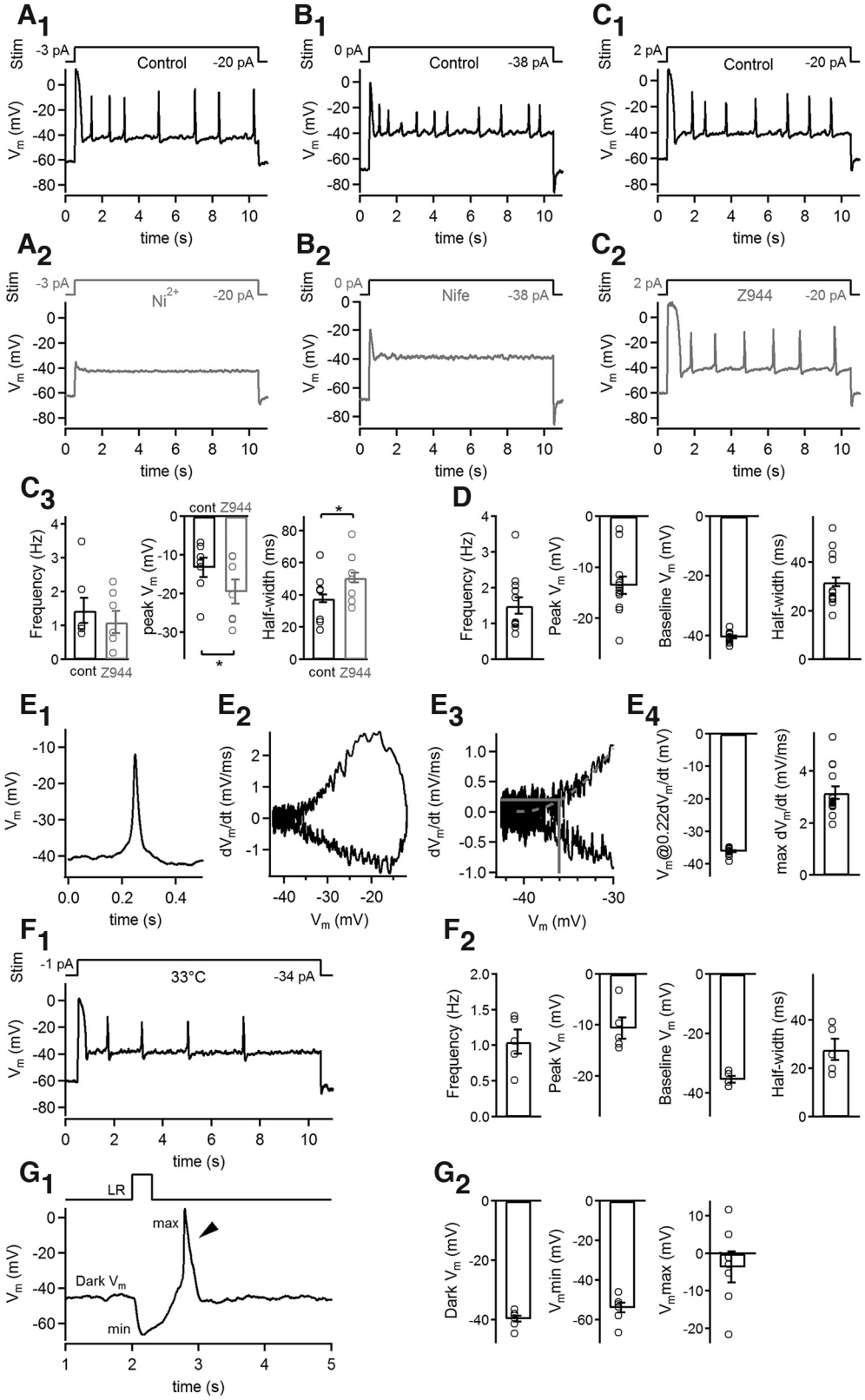

Figure 5. Spontaneous spike activity at dark V_m. ***A1–C2***, Example V_m changes in control condition and during 100 μM nickel (Ni^{2+}), 10 μM nifedipine (Nife), and 5 μM Z944 application. ***C3***, Peak V_m of spontaneous spike events: control, −13.3 ± 2.50 mV; Z944, −19.45 ± 3.13 mV; $n = 7$; $p = 0.0337$, paired t test. Spontaneous spike frequency: control, 1.45 ± 0.38 Hz; Z944, 1.1 ± 0.32 Hz; $n = 7$; $p = 0.2462$, paired t test. Half-width: control, 38.0 ± 2.50 ms; Z944, 50.68 ± 3.13 ms; $p = 0.0145$, paired t test; $n = 7$. ***D***, Summary of spike parameters generated in control condition. Frequency, 1.47 ± 0.23; peak V_m, −13.56 ± 1.72 mV; baseline V_m, −40. 57 ± 0.50 mV; half-width, 31.96 ± 1.72 ms. ***E1***, Example of a spontaneous spike in cone photoreceptors. ***E2***, Time derivative of the V_m of the trace in ***E1*** plotted against V_m. ***E3***, Zoomed in region of the rising phase from ***E2***. Dashed gray line, Exponential fit to estimate the average of the trace; straight gray lines, 7.5% of the maximal rise rate reveals the V_m threshold of the spike. ***E4***, V_m at 0.22 dV/dt: −36.17 ± 0.29 mV; $n = 14$; maximal V_m rise rate: 3.17 ± 0.24 mV/ms; $n = 14$. ***F1***, Example V_m changes at near body temperature (33°C). ***F2***, Frequency of spikes, 1.05 ± 0.17 Hz; peak V_m, −10.65 ± 2.05 mV; baseline, −35.52 ± 1.1 mV; half-width, 27.77 ± 4.3 ms. Room temperature versus 33°C: frequency, $p = 0.2610$; peak V_m, $p = 0.3458$; baseline, $p = 0.0002$; half-width, $p = 0.4844$, unpaired t test; $n = 12$ and $n = 5$, respectively. ***G1***,

spike behavior near body temperature (33°C; Fig. 5*F1*,*F2*). Spontaneous spikes were also evoked at higher temperature by current injection values that were used during the experiments in room temperature (room temperature, -1.41 ± 0.74 pA; 33°C, -2.8 ± 1.02 pA; $p = 0.1349$, $n = 12$ and $n = 5$, respectively, unpaired t test). We also tested whether spikes could be generated by natural stimuli. We performed current-clamp ($I = 0$) experiments in dark-adapted retinae using dim red light during slicing and recording. Full-field light flashes (irradiance, ~130 W/cm^2) evoked a typical light response in cone photoreceptors and an additional spike at light offset (Fig. 5*G1*). Cone photoreceptors initially stayed at V_m = approximately −39 mV (Fig. 5*G1*, Dark V_m), then the light flash induced a fast hyperpolarization to approximately −54 mV (Fig. 5*G2*, V_{min}). Spikes evoked by light offset reached a peak approximately V_m = 0 mV (V_{max}), as observed for spikes generated by current injections (Fig. 4, controls). These experiments illustrate that mouse cone photoreceptors generate Ca^{2+} spikes in dark and at light offset. Therefore, cone photoreceptors seem to process light information by both gradual V_m change and spike generation.

Spike activity increases intracellular Ca^{2+} levels in cone photoreceptor terminals

We showed that cone photoreceptors are able to generate spikes in response to a V_m jump and spontaneously at depolarized V_m and provided pharmacological evidence that spikes were produced by the activation of voltage-sensitive T-type and L-type Ca^{2+} channels. Here, we wanted to further investigate whether spikes stimulate the influx of Ca^{2+} into the cone photoreceptor terminal. Therefore, to detect spatially averaged intracellular Ca^{2+} changes, we used 100 µM Fluo-4 Ca^{2+} indicator (Thermo Fisher Scientific) in the pipette solution. Fluo-4 has been shown to be sufficiently sensitive (K_d = 345 nM) to detect low concentrations of free intracellular Ca^{2+} (Gee et al., 2000). In the experiments, we targeted cone photoreceptor terminals in the horizontal retina slice preparation with the patch electrodes and measured Ca^{2+} signals parallel to current-clamp measurements. First, we injected negative currents to keep the cells at hyperpolarized V_m, then we injected positive currents to depolarize the cells to a level that is close to the threshold of spike generation (approximately −40 mV). Figure 6*A* shows an example of a cone photoreceptor held at approximately −80 mV by injecting −13 pA current followed by a V_m step to more positive values for 5 s by injecting −4 pA current. In this example, the cone photoreceptor showed spikes at the start of the stimulation but shortly after (~2 s), V_m remained steady at approximately −50 mV without spikes (Fig. 6*A*, black trace). The V_m of −50 mV is more negative than the activation threshold of the T-type Ca^{2+} channels (approximately −40 mV). Accordingly, intracellular Ca^{2+} concentration ($\Delta F/F_0$) rose at the start of the stimulus and then declined slowly to baseline values. This indicates that the current injection activated voltage-sensitive Ca^{2+} channels at the beginning of the stimulus, which resulted in an intracellular Ca^{2+} rise in the terminal, but because of the absence of further spike generation at −50 mV, Ca^{2+} was slowly removed from the terminal. In the next example, V_m was changed to a more depolarized level by a current step to −2 pA (Fig. 6*B*). During the presence of this depolarizing current, V_m of the cone photoreceptor showed continuous spike activity at ~1 Hz, and Ca^{2+} signals were elevated to a steady level. Additionally, because of the spike activity, a clear concurrent rise of the Ca^{2+} signal was observed (Fig. 6*B*, arrows). The relationship between spikes and intracellular Ca^{2+} concentration was analyzed by measuring the linear correlation between spike timing and Ca^{2+} signal peaks (Fig. 6*C*). We found a significant correlation ($p < 0.0001$, $R^2 = 0.9992$), indicating that spikes were generated by Ca^{2+}. We found an average $\Delta F/F_0$ of 1, and the Ca^{2+} signal peak could be detected ~30 ms after spike peaks (Fig. 6*D*). Altogether, these experiments show that during self-generating spike activity at around dark V_m, the intracellular Ca^{2+} concentration rises from baseline level and stays at a steady high level, while individual spikes can further increase Ca^{2+} levels temporarily in cone photoreceptor terminals. Additionally, the local Ca^{2+} concentration rise suggests that both T-type and L-type Ca^{2+} channels localize at the cone photoreceptor terminal membrane.

Both LVA and HVA Ca^{2+} channels contribute to synaptic vesicle release

To investigate the role of LVA T-type Ca^{2+} channels in synaptic vesicle release, first, we took advantage of the biophysical properties of the channels. At depolarized V_m (−41 mV), I_{LVA} showed partial (~46%) inactivation, but I_{HVA} inactivation was only ~15% (Fig. 3). We therefore, compared synaptic vesicle release evoked by a test stimulus (−19 mV, 25 ms) preceded by an ~15-s-long, either hyperpolarized (V_h = −69 mV; Fig. 7*A1*, black) or depolarized (V_h = −39 mV, Fig. 7*A1*, gray) potential. Evoked synaptic vesicle release in cone photoreceptors was monitored by C_m measurements with the Sine + DC method (HEKA 10 Amplifier, HEKA Elektronik). We found that I_{Ca} charge (QI_{Ca}) was ~1.5 pC in the presence of LVA and HVA Ca^{2+} channels (V_m = −69 mV). When V_m was held at −39 mV, QI_{Ca} decreased to ~0.8 pC, significantly diminishing evoked synaptic vesicle release (Fig. 7*A2*). The number of released synaptic vesicles in cone photoreceptors was estimated by taking into account the single synaptic vesicle capacitance contribution, which has a typical value of 43.7 aF in mouse photoreceptors based on a 37.3 nm synaptic vesicle diameter (Fuchs et al., 2014). This yields ~1730 synaptic vesicles at V_h = −69 mV and ~1030 synaptic vesicles at V_h = −39 mV; thus, ~41% fewer synaptic vesicles were released by the inactivation of LVA T-type Ca^{2+} channels. This result indicates that LVA T-type Ca^{2+} channels contribute to Ca^{2+}-dependent synaptic vesicle release at cone photoreceptors. Next, we examined the contribution of HVA L-type Ca^{2+} channels to evoked synaptic vesicle release by the application of 10 µM nifedipine that reduced I_{HVA} by ~68% and left I_{LVA} unaltered (Fig. 2*E1*,*E2*). Synaptic vesicle release was triggered by a test pulse (−19 mV, 25 ms) from V_h = −69 mV (Fig. 7*B1*), and nifedipine was applied with a pressure-controlled puffing system. QI_{Ca} showed a significant, ~49%, reduction in the presence of 10 µM nifedipine, but evoked synaptic vesicle release was only reduced by ~16% (Fig. 7*B2*). This result indicates that LVA T-type Ca^{2+} channels contribute more to synaptic vesicle release than HVA L-type Ca^{2+} channels (Fig. 7*A1*) and therefore have a boosting effect on synaptic vesicle release evoked by a strong stimulus (−19 mV, 25 ms) at mouse cone photoreceptors. As this is an unexpected finding, we further examined the effect of LVA T-type Ca^{2+} channels on synaptic vesicle release at cone photoreceptors. In the following experiments, we included 10 mM bis(2-aminophenoxy)ethane-*N*,*N*,*N*′,*N*′-tetra-acetic acid (BAPTA) in

←

Example trace showing V_m changes evoked by full-field light flash (300 ms, ~130 W/cm^2 irradiance) in dark-adapted cone photoreceptor. G_2, V_m before light stimulation (Dark V_m), −39.65 ± 0.99 mV; light response evoked V_m hyperpolarization (V_{min}), −53.96 ± 2.46 mV; offset of the light response (V_{max}), −3.61 ± 4.08 mV.

the pipette solution. BAPTA is a Ca^{2+} buffer with a faster on-rate than EGTA has, intercepting Ca^{2+} influx at the active zone via Ca^{2+} channels to reveal nanodomain or microdomain organization (Adler et al., 1991). The presence of BAPTA in the pipette did not change QI_{Ca} compared with EGTA (5 mM EGTA; Fig. 7*B*, black: QI_{Ca} = 1.16 ± 0.19 pC, n = 6; 10 mM BAPTA; Fig. 7*C*, black: QI_{Ca} = 1.28 ± 0.10 pC, n = 5, p = 0.6236, unpaired t test). However, 10 mM BAPTA caused a significant reduction in ΔC_m (5 mM EGTA, Fig. 7*B*, black: 90.00 ± 10.73 pC, n = 6; 10 mM BAPTA, Fig. 7*C*, black: 35.16 ± 5.18 pC, n = 5, p = 0.0018, unpaired t test). The ~61% reduction of C_m indicates that most of the evoked synaptic vesicle release was triggered by Ca^{2+} influx through nanodomain-organized Ca^{2+} channels. Moreover, 39% of the evoked synaptic vesicle release in cone photoreceptors is either not sensitive to BAPTA or is Ca^{2+} independent. Nifedipine application, in the presence of BAPTA, caused a reduction of QI_{Ca} (Fig. 7*C2*) similar to what we observed with the EGTA-containing intracellular solution (Fig. 7*B2*). However, ΔC_m values decreased by ~48% in the presence of the fast Ca^{2+} buffer (Fig. 7*C2*), which exceeded the degree of reduction that we measured in the presence of 5 mM EGTA (~16%; Fig. 7*B2*). The stronger nifedipine sensitivity of the release in the presence of BAPTA indicates that most of the HVA L-type Ca^{2+} channels are organized into nanodomains at the active zone (Bartoletti et al., 2011). Moreover, the smaller nifedipine sensitivity in the presence of EGTA (Fig. 7*B*,*C*, gray) suggests that LVA T-type Ca^{2+} channels provide an additional Ca^{2+} source to trigger and boost synaptic vesicle release and that they locate close to the release sites. The mild stimuli evoked QI_{Ca} in the presence of 5 mM EGTA and 10 mM BAPTA reached similar values, but the synaptic vesicle release was significantly different (Fig. 7*D*). The reduced ΔC_m levels with BAPTA and the maintained ΔC_m levels with EGTA further strengthen the finding that LVA T-type channels are present close to the release sites and are able to boost synaptic vesicle release. To further examine the boosting effect of LVA T-type Ca^{2+} channels, we measured cone photoreceptor synaptic vesicle release in response to mild (−39 mV, 25 ms) and strong (−19 mV, 25 ms) depolarizing steps. Stimuli were applied pairwise to the same cone photoreceptor using a pipette solution containing either 5 mM EGTA or 10 mM BAPTA (Fig. 7*E*,*F*). At V_m = approximately −39 mV, the LVA T-type Ca^{2+} current has a maximal amplitude, while HVA L-type Ca^{2+} channels are activated only slightly (Figs. 1, 3). Consequently, mild stimulation should activate mainly LVA T-type Ca^{2+} channels, and strong stimulation should activate both Ca^{2+} channel types. We found that a mild stimulus significantly diminished QI_{Ca} compared with the strong stimulus in both Ca^{2+} buffering conditions (Fig. 7*E*,*F*). However, in the presence of 5 mM EGTA, the mild stimulus reduced synaptic vesicle release by only ~12% (Fig. 7*E*), which is consistent with the result shown in Figure 7*B*, where mainly LVA T-type Ca^{2+} channels dominated evoked synaptic vesicle release. This shows that LVA T-type Ca^{2+} channels are capable of triggering synaptic vesicle release with high efficiency (~88%) when photoreceptors are quickly depolarized from the light to the dark membrane potential (−39 mV). On the other hand, the comparison of mild and strong depolarization steps in the presence of 10 mM BAPTA revealed an

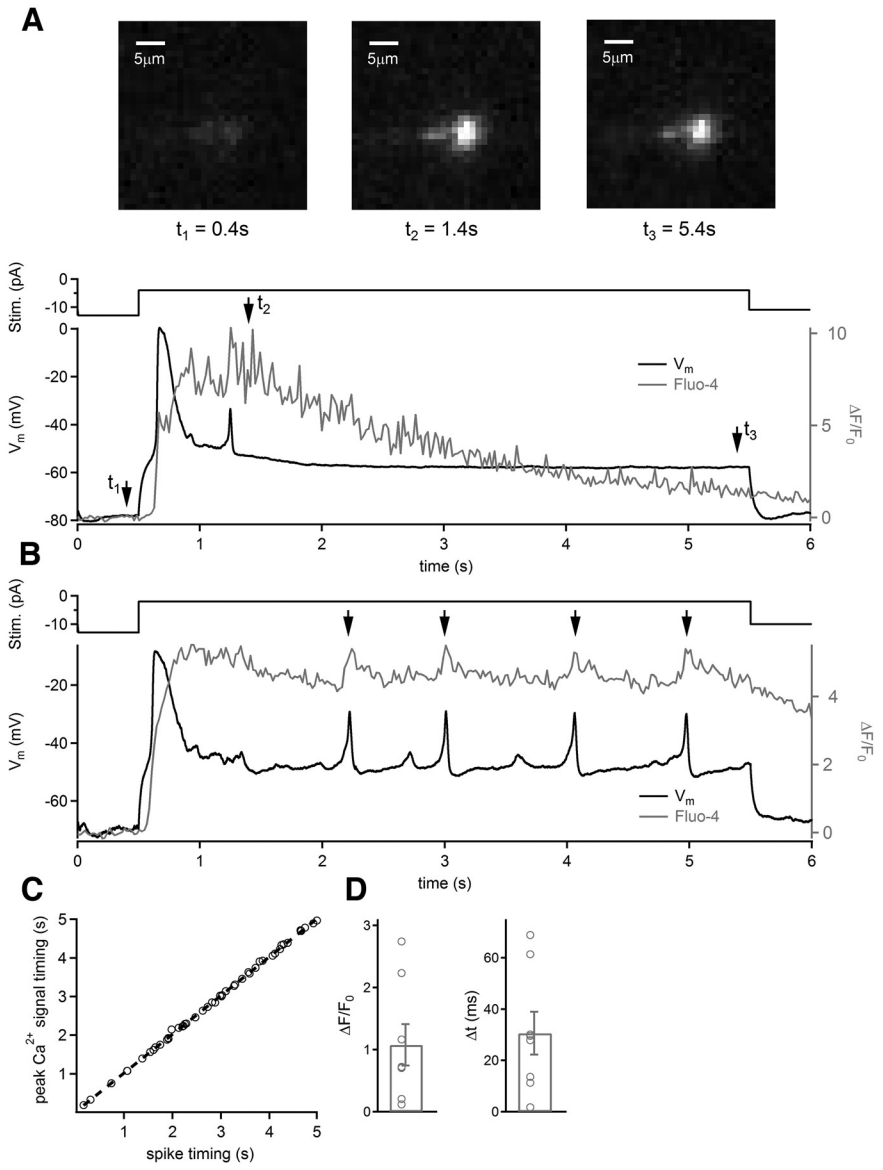

Figure 6. Spikes cause intracellular Ca^{2+} rise in cone photoreceptor terminals. ***A***, Example of simultaneous current-clamp recording (from −13 to −4 pA, 5 s) and Ca^{2+} imaging with 100 µM Fluo-4 in the cone photoreceptor terminal. Pictures in the top panel were taken from the patched cone photoreceptor terminal at the time points labeled with arrows (t_1–t_3). ***B***, Example of simultaneous current-clamp recording and Ca^{2+} imaging during stronger stimulation (from −13 to −2 pA, 5 s). Arrows indicate Ca^{2+} rise because of the individual spike events. ***C***, Linear relationships between the timing of spike and Ca^{2+} signal peak ($p < 0.0001$, $R^2 = 0.9992$). ***D***, Relative Ca^{2+} change during spikes ($\Delta F/F_0$), 1.08 ± 0.33; Δt between spike peak amplitude and Ca^{2+} signal peak (Δt), 30.58 ± 8.36 ms.

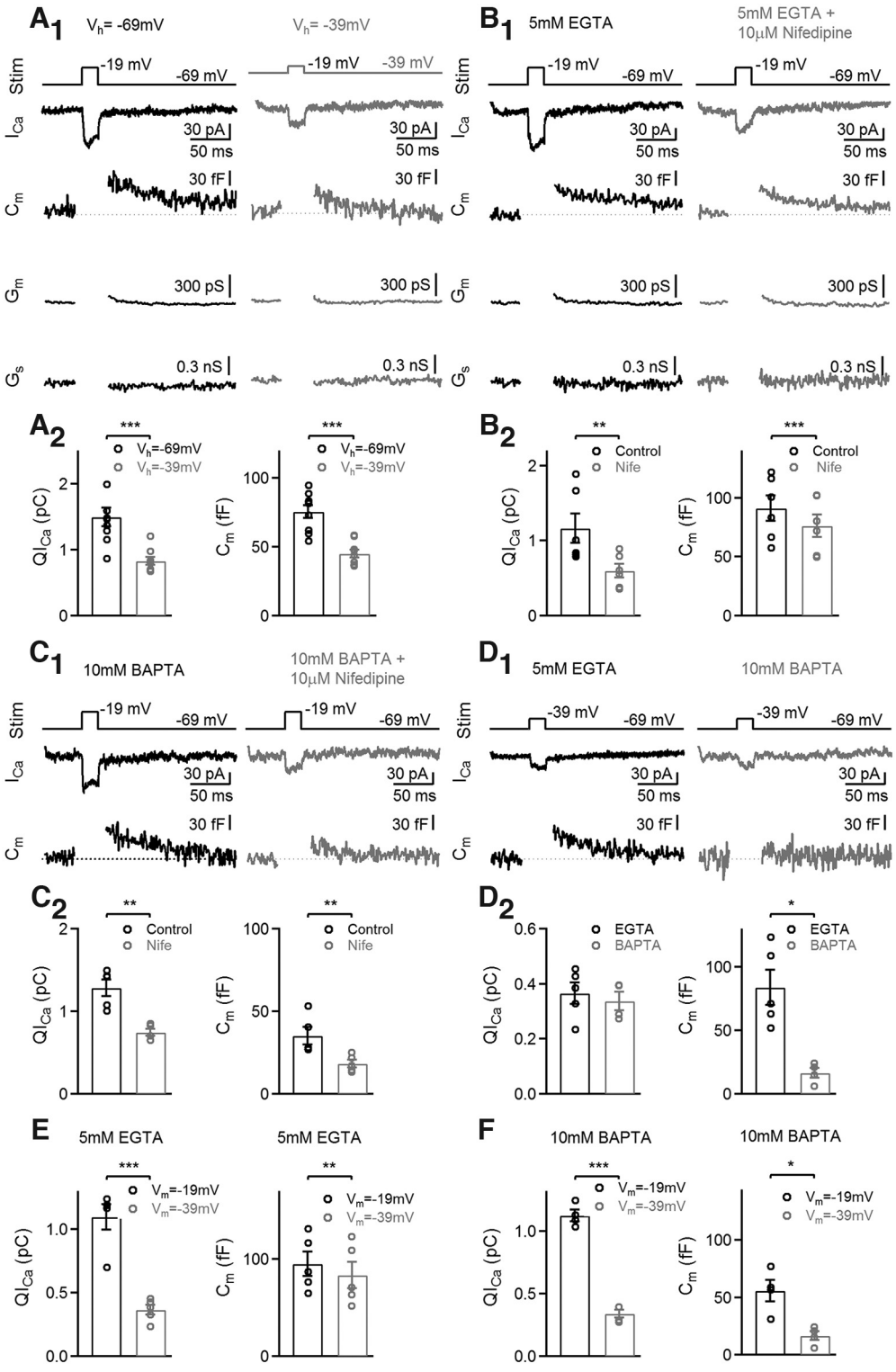

Figure 7. LVA Ca^{2+} channels boost synaptic vesicle release. ***A*$_1$**, Black, Example traces showing I_{Ca} and C_m induced by a voltage step (from −69 to −19 mV, 25 ms) at cone photoreceptors. Stim, Stimulus; G_m, membrane conductance; G_s, series conductance; gray, I_{Ca} and C_m induced by a voltage step (from −39 to −19 mV, 25 ms). Labeling similar to black traces. ***A*$_2$**, QI_{Ca}: V_h = −69 mV: 1.35 ± 0.19 pC; V_h = −39 mV: 0.83 ± 0.06 pC; $n = 7$; $p = 0.0003$, paired t test; C_m: V_h = −69 mV: 75.62 ± 4.69 fF; V_h = −39 mV: 45.02 ± 2.90 fC; $n = 7$; $p = 0.0003$, paired t test. ***B*$_1$**, Black, Example traces of I_{Ca} and C_m jump induced by voltage stimulus (from −69 to −19 mV, 25 ms), Patch pipette contained 5 mM EGTA. Gray, Same as black but in the presence of 10 μM nifedipine. ***B*$_2$**, QI_{Ca}: control, 1.16 ± 0.19 pC; Nife, 0.59 ± 0.09 pC; $n = 6$; $p = 0.0047$, paired t test; C_m: control, 90.99 ± 10.73 fF; Nife, 76.23 ± 9.52 fF; $n = 6$; $p = 0.0007$, paired t test. ***C*$_1$**, Black, Example traces of I_{Ca} and C_m change induced by a voltage step (from −69 to −19 mV, 25 ms). Pipette contained 10 mM BAPTA. Gray, Same as black but in the presence of 10 μM nifedipine. ***C*$_2$**, QI_{Ca}: control: 1.28 ± 0.10 pC, $n = 5$; Nife: 0.74 ± 0.04 pC, $n = 5$; $p = 0.0021$, paired t test; C_m: control: 35.16 ± 5.18 fF, $n = 5$; Nife: 18.45 ± 2.23 fF, $n = 5$; $p = 0.0063$, paired t test. ***D*$_1$**, Black, Example traces of I_{Ca} and C_m jump induced by a voltage step (from −69 to −39 mV, 25 ms). Pipette contained 5 mM EGTA. Gray, Same as black but with 10 mM BAPTA-containing intracellular solution. ***D*$_2$**, QI_{Ca}: 5 mM EGTA, 0.36 ± 0.04 pC; 10 mM BAPTA, 0.34 ± 0.03 pC; $n = 5$ and $n = 4$; $p = 0.7302$, unpaired t test; C_m: 5 mM EGTA, 83.68 ± 13.76 fF; 10 mM BAPTA, 16.61 ± 3.99 fF; $n = 5$ and $n = 4$; $p = 0.0159$, unpaired t test. ***E***, Paired comparison of (−19 mV, 25 ms; strong) and mild (−39 mV, 25 ms; mild) stimulus evoked QI_{Ca} with 5 mM EGTA containing intracellular solution. Mild, QI_{Ca} = 0.36 ± 0.04 pC; strong, QI_{Ca} = 1.09 ± 0.1 pC; $n = 5$; $p = 0.0005$, paired t test. Mild, ΔC_m = 83.68 ± 13.76 fF; strong, ΔC_m =

~70% difference in evoked synaptic vesicle release (Fig. 7*F*). This demonstrates that LVA T-type Ca^{2+} channels are less effective in boosting synaptic vesicle release when the fast Ca^{2+} buffer is present; hence, they likely locate close to HVA L-type Ca^{2+} channels.

Cone photoreceptors express $Ca_v3.2$ channel mRNA

To investigate which LVA T-type Ca^{2+} channels are present in cone photoreceptors, we performed RT-PCR experiments on sorted rod and cone photoreceptors from dissociated retinae of Rac3-eGFP mice, which express eGFP in cone photoreceptors (Gong et al., 2003; Fuchs et al., 2014). For fluorescence-activated cell sorting, eGFP fluorescence and FSC/SSC were used to sort cone and rod photoreceptors, respectively (Fig. 8*A1*,*A2*). The unlabeled sorting of rod photoreceptors by FSC/SSC is possible because of the high backscatter of heterochromatin in adult rod photoreceptor somata (Solovei et al., 2009; Feodorova et al., 2015). This method was optimized and validated by the use of CD73, a cell surface marker of cone/rod photoreceptor common precursors and mature rod photoreceptors (Koso et al., 2009). We performed nested RT-PCR with primers that have been validated and successfully deployed on mouse islet cDNA (Vignali et al., 2006). The results of the nested RT-PCR of sorted photoreceptors indicate that cone photoreceptors express $Ca_v3.2$, whereas rod photoreceptors do not express any LVA T-type Ca^{2+} channel (Fig. 8*B1*). To verify our sorting strategy, we also checked for the expression of β-actin (Actb), the cone photoreceptor marker short-wave-sensitive opsin 1 (Opn1sw), and the rod photoreceptor marker rhodopsin (Rho; Fig. 8*B2*). While Actb was present in all analyzed samples, Opn1sw was enriched in cone photoreceptors and Rho in rod photoreceptors, corroborating our sorting strategy (Fig. 8*B2*). On whole-retina cDNA, application of the primers led to specific bands for all three LVA T-type Ca^{2+} channels $Ca_v3.1$ (271 bp), $Ca_v3.2$ (305 bp), and $Ca_v3.3$ (258 bp; Fig. 8*C1*), as well as for the markers Actb (196 bp), Opn1sw (175 bp), and Rho (81 bp; Fig. 8*C2*). No bands were detectable in the negative control, in which reverse transcriptase was omitted during cDNA synthesis of whole-retina mRNA, to exclude amplification of genomic DNA (Fig. 8*C1*,*C2*). This confirms the nested RT-PCR results and demonstrates the mRNA expression of $Ca_v3.2$ in cone photoreceptors. Furthermore, data of previous work using "Drop-Seq" analysis of individual cells also suggests the presence of $Ca_v3.2$ mRNA in cone photoreceptors (Macosko et al., 2015).

Discussion

LVA and HVA I_{ca} in cone photoreceptors

There is good anatomic and functional evidence for the presence of $Ca_v1.3$ and/or $Ca_v1.4$ L-type Ca^{2+} channels in mammalian photoreceptors (Dieck et al., 2005; Mansergh et al., 2005; Morgans et al., 2005; Wu et al., 2007; Xiao et al., 2007; Regus-Leidig et al., 2014a). To the best of our knowledge, there is so far no evidence for the presence of non-L-type Ca^{2+} channels in photoreceptors. A previous study, which described the membrane conductances of mouse cone photoreceptors showed evidence for only L-type Ca^{2+} currents (Ingram et al., 2020). In this work, Ames' Medium was used as an extracellular solution. Ames' Medium contains among others ascorbic acid, which blocks T-type Ca^{2+} currents (Nelson et al., 2007), and the intracellular solution contained QX-314-Br, which blocks LVA Ca^{2+} currents (Talbot and Sayer, 1996).

Here, we provide functional and structural evidence by directly targeting mouse cone photoreceptor terminals by patch pipettes of ~10 MΩ resistance that the measured I_{LVA} is most likely produced by T-type Ca^{2+} channels. First, T-type Ca^{2+} channel antagonists such as nickel and Z944 significantly blocked I_{LVA}. Second, physiological parameters of pharmacologically isolated I_{LVA} analyzed in Figure 3 were similar to reported values for T-type Ca^{2+} channels in heterologous expression systems (Klöckner et al., 1999; Perez-Reyes, 2003). Third, spikes coincide with increased Ca^{2+} levels in the synaptic terminal. Moreover, RT-PCR experiments revealed the presence of $Ca_v3.2$ but not $Ca_v3.1$ or $Ca_v3.3$ T-type Ca^{2+} channel mRNA in FACS sorted cone photoreceptors. Nevertheless, and despite the use of a wide variety of pharmacological tools to isolate Ca^{2+} currents in cone photoreceptors, we cannot fully exclude the contribution of other ion conductances to our measurements. For example, the presence of TTX-resistant $Na_v1.9$ channels in photoreceptors was shown by immunolabeling (O'Brien et al., 2008). However, $Na_v1.9$ channels start to activate at hyperpolarized potentials (approximately −80 mV) and show ultraslow inactivation kinetics (Dib-Hajj et al., 2015; Lin et al., 2016), which is different from the I_{LVA} kinetics reported in this work. In our experiments, I_{LVA} of cone photoreceptors was not sensitive to blockers of TTX-sensitive Na^+ channels, hyperpolarization-activated channels, or N-type Ca^{2+} channels, excluding these ion channels as contributors to I_{LVA}.

LVA Ca^{2+} channels are also called T-type Ca^{2+} channels referring to their physiological properties, displaying a transient and tiny current. Based on their physiological properties, the different isoforms of T-type Ca^{2+} channels are indistinguishable because their activation and inactivation parameters taken from the Boltzmann equation are similar (Klöckner et al., 1999). In our experiment, I_{HVA} peaked at approximately −20 mV, which is relatively far from the dark-induced V_m change in photoreceptors but I_{LVA} started to activate at approximately −50 mV and showed a peak current at approximately −40 mV, which is in the range of the typical light-generated V_m change (from −70 to −40 mV). This indicates that the light-induced V_m change first activates LVA T-type Ca^{2+} channels followed by HVA L-type Ca^{2+} channels; thereby, synaptic vesicle release with light-induced V_m change could be connected. Another mechanism to overcome the misalignment between the L-type Ca^{2+} channel activation range and the light-evoked V_m change is the Ca^{2+} influx through cGMP channels in salamander cone photoreceptors, which contributes to neurotransmitter release (Rieke and Schwartz, 1994). I_{LVA} would appear to lessen the need for such a mechanism in mouse cone photoreceptors. The pharmacological identification of LVA T-type Ca^{2+} channels is not straightforward in the presence of HVA L-type Ca^{2+} channels. At concentrations used to block LVA T-type Ca^{2+} channels, compounds such as ethosuximide (Coulter et al., 1989) and amiloride (Tang et al., 1988) also affect other types of Ca^{2+} channels. Mibefradil, a commonly used LVA T-type Ca^{2+} channel blocker also inhibits HVA L-type Ca^{2+} channels (Leuranguer et al., 2001; Lee et al., 2006; To et al., 2020). The small but not significant effect of 1 μM mibefradil on I_{LVA} and I_{HVA} and the opposing effect of 5 μM Z944 on I_{LVA} and

←

95.24 + 12.42 fF; $n = 5$; $p = 0.0021$, paired t test. ***F***, Paired comparison of strong (−19 mV, 25 ms) and mild (−39 mV, 25 ms) stimulus-evoked Q_{Ca} with 10 mM BAPTA containing intracellular solution. Mild: $Q_{Ca} = 0.33 \pm 0.03$ pC; strong: $Q_{Ca} = 1.12 \pm 0.04$ pC; $n = 4$; $p = 0.0005$, paired t test; mild: $\Delta C_m = 16.61 \pm 3.99$ fF; $p = 0.0005$; strong: $\Delta C_m = 55.97 \pm 9.44$ fF; $n = 4$; $p = 0.01$, paired t test.

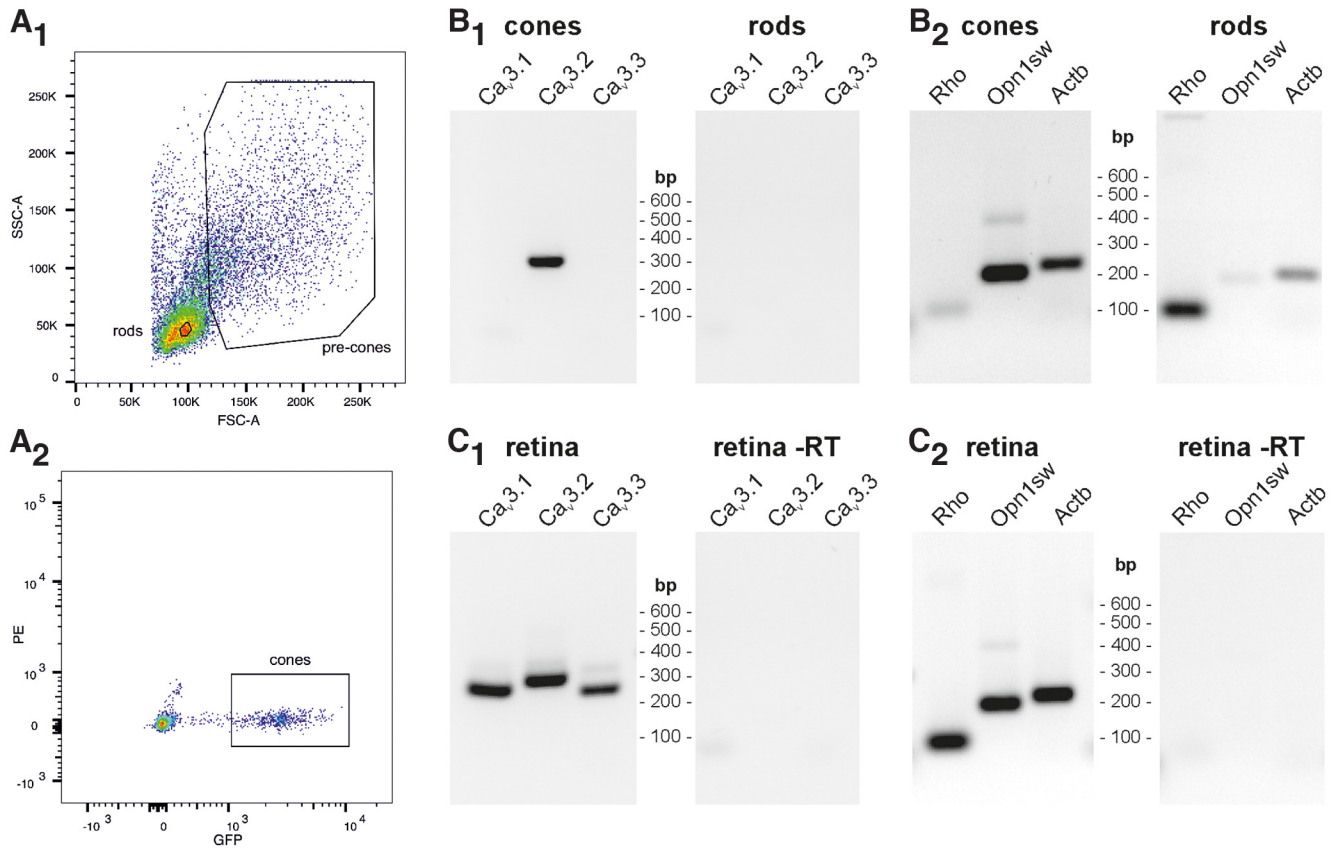

Figure 8. Analysis of T-type Ca^{2+} channels in sorted photoreceptors. ***A1***, FACS strategy for isolating rod photoreceptors by FSC/SSC. ***A2***, FACS strategy for isolating cone photoreceptors by GFP fluorescence of Rac3-eGFP mice. ***B1***, Nested RT-PCR analysis of sorted cone and rod photoreceptor samples with LVA-specific primer pairs for $Ca_v3.1$, $Ca_v3.2$, and $Ca_v3.3$. A distinct band is present for the cone photoreceptor sample using $Ca_v3.2$ primers, whereas no bands can be observed for the sorted rod photoreceptor population. ***B2***, Conventional RT-PCR with primers for Rho, Opn1sw, and Actb on sorted rod and cone photoreceptors. Strong bands are visible for Opn1sw and Rho in cone and rod photoreceptor samples, respectively, as well as for Actb. ***C1***, ***C2***, RT-PCR analysis of whole-retina and negative control samples, in which reverse transcriptase was omitted during cDNA synthesis (retina, −RT). For whole retina, the following expected bands are present: $Ca_v3.1$ (271 bp), $Ca_v3.2$ (305 bp), $Ca_v3.3$ (258 bp), Rho (81 bp), Opn1sw (175 bp), and Actb (196 bp). No bands are visible for retina −RT samples.

I_{HVA} (Fig. 2) suggest that HVA L- and LVA T-type Ca^{2+} channels in mouse cone photoreceptors have unique molecular properties. Several unique isoforms of synaptic proteins have already been reported for photoreceptors such as Piccolino (Regus-Leidig et al., 2013, 2014b), complexin 4 (Reim et al., 2005, 2009), and syntaxin 3B (Morgans et al., 1996; Curtis et al., 2008). Nickel is a divalent cation that preferentially inhibits the LVA T-type Ca^{2+} channel $Ca_v3.2$ at low micromolar concentrations (Lee et al., 1999). It significantly blocked I_{LVA} in our experiments (Fig. 2). The partial block of I_{HVA} by nickel is consistent with the findings that nickel also blocks HVA L-type Ca^{2+} channels (McFarlane and Gilly, 1998; Hobai et al., 2000; To et al., 2020). In general, the results of the pharmacological experiments indicate that the LVA Ca^{2+} channels in mouse cone photoreceptors are LVA T-type Ca^{2+} channels and not hyperpolarization-activated channels or TTX-sensitive Na^+ or N-type Ca^{2+} channels (Fig. 2). RT-PCR experiments on sorted cone photoreceptors propose that T-type Ca^{2+} channels, present at cone photoreceptors, are the $Ca_v3.2$ channel and not the $Ca_v3.1$ or $Ca_v3.3$ channel (Fig. 8).

Spiking photoreceptors

Mammalian photoreceptors are generally characterized as nonspiking neurons (Yagi and Macleish, 1994; Schneeweis and Schnapf, 1995; Ingram et al., 2020). However, toad rod, turtle cone, and lizard cone photoreceptors can generate Ca^{2+} spikes (Fain et al., 1980; Gerschenfeld et al., 1980; Maricq and Korenbrot, 1988). Cone photoreceptors showed fast spike-like currents occasionally in premortem and postmortem monkey retina (Bryman et al., 2020). Furthermore, spikes and biphasic light responses were also observed in monkey photoreceptors in another study (Schnapf et al., 1990). However, spike-like currents and biphasic light responses were not observed in a more recent work, suggesting that spikes at monkey photoreceptors might be caused by tissue degradation (Cao et al., 2014). Cultured human rod and cone photoreceptors have been shown to express voltage-gated Na^+ channels and generate action potentials sensitive to TTX (Kawai et al., 2001, 2005). However, spike generation in human photoreceptors required that they be held at a highly hyperpolarized V_m (approximately −80 mV), which is more negative than the V_m normally attained in bright light (approximately −70 mV), and spikes were observed only in unhealthy tissue. This indicates that action potentials in human photoreceptors might be because of the experimental conditions and may not appear under physiological conditions (Van Hook et al., 2019). Light-evoked Ca^{2+} spikes in dark-adapted goldfish ON bipolar cells have also been observed (Protti et al., 2000); however, here the block of L-type Ca^{2+} channels caused periodic spiking different from our observation when nifedipine blocked spike generation (Fig. 5). The spikes emerging at light offset might enhance the contrast detection at cone photoreceptors between dark and light. This is similar to retinal bipolar cell behavior where small signals are accelerated and amplified by T-type Ca^{2+} channels (Protti et al., 2000). In our experiment, the

observed continuous spiking activity at approximately −40 mV did not require a preceding period of hyperpolarization of the cone photoreceptor membrane (Fig. 5), indicating that the spike generation could play a role in the information transfer at constant light levels. Furthermore, photoreceptor light responses could be converted to both sustained and transient components, which led to increased intracellular Ca^{2+} levels in the synaptic terminal (Fig. 6). This could trigger several Ca^{2+}-dependent processes such as the activation of Ca^{2+}-induced Ca^{2+} release, the activation of Ca^{2+}-dependent Cl^- and K^+ channels, the acceleration of synaptic vesicle replenishment, alterations in the local driving force for Ca^{2+}, as well as controlling synaptic vesicle release kinetics.

Action potentials are generally associated with the spread of depolarizing signals along the axon. Mouse cone photoreceptors have a relatively short, ~50-µm-long axon. The impact of axon properties showed little effect on the passive signal weakening between the soma and terminal of a bipolar cell, which has an axon length that is 1.5 times longer than that of cone photoreceptors (Oltedal et al., 2009). Consequently, a shorter cone photoreceptor axon should have an even smaller effect on the passive signal spread. In numerous neurons, T-type Ca^{2+} channels generate low-threshold spikes, which in turn trigger the activation of Na^+ channels and thereby a burst of action potentials and oscillatory behavior (Huguenard, 1996; Perez-Reyes, 2003). We measured the sensitivity of Ca^{2+} currents and spikes to 1 µM TTX, which did not affect Ca^{2+} current or spike amplitude. $Na_v1.9$ channels usually do not generate spikes; they rather act as a threshold channel (Herzog et al., 2001; Osorio et al., 2014). The results of our experiments suggest that spikes at cone photoreceptors are generated by T- and L-type Ca^{2+} channels. Ca^{2+} spikes are not uncommon in biological systems. For example, L-type Ca^{2+} channels trigger spikes in dopamine neurons with a 0.5 mV/ms rise rate (Iyer et al., 2017) and T-type Ca^{2+} channels trigger spikes in several neuron types reviewed in the study by Perez-Reyes (2003).

Inferences of the function of LVA T-type Ca^{2+} channels in cone photoreceptors

Neurotransmitter release at ribbon synapses has been generally attributed to only HVA L-type Ca^{2+} channels. For example, the ribbon containing auditory hair cells in the bullfrog amphibian papilla, which also express both T- and L-type Ca^{2+} channels, did not show any synaptic vesicle release during the pharmacological block of L-type Ca^{2+} channels (Cho and von Gersdorff, 2014). However, several studies have reported a key role for LVA Ca^{2+} channels in neurotransmitter release and hormone secretion in neuronal tissues (Angstadt and Calabrese, 1991; Tang et al., 2011), and also for retinal neurons other than photoreceptors, such as salamander ganglion cells (Henderson and Miller, 2007), mouse horizontal cells (Feigenspan et al., 2020), and rat bipolar cells (Pan, 2000; Pan et al., 2001). Furthermore, LVA Ca^{2+} channels directly triggered exocytosis in ribbon-containing synapses such as retinal bipolar cells (Kaneko et al., 1989; Pan et al., 2001). In addition, in developing chicken basilar papilla auditory hair cells, the temporal characteristics of Ca^{2+} entry through LVA T-type and HVA L-type Ca^{2+} channels greatly influenced synaptic release (Levic and Dulon, 2012). Interestingly, neurotransmission at photoreceptor ribbon synapses is much more sensitive to Ca^{2+} than at conventional synapses (Mercer and Thoreson, 2011); however, both synapse types use synaptotagmin-1 as a Ca^{2+} sensor (Grassmeyer et al., 2019). We show evidence that cone photoreceptors use two Ca^{2+} sources, namely LVA L-type and HVA T-type Ca^{2+} channels, which activate at different voltage ranges, have different amplitudes, and localize close to the release site. Therefore, the use of both Ca^{2+} channel types could contribute to the adjustment of high Ca^{2+} sensitivity of the release machinery.

Because the detection of bright, high-frequency visual signals requires both presynaptic and postsynaptic mechanisms (Grabner et al., 2016), the use of LVA and HVA Ca^{2+} channels in both presynaptic (cone photoreceptors) and postsynaptic neurons (horizontal and bipolar cells) might increase the visual signal processing capacity of the retina by giving greater dimension in the gain and kinetics of synaptic signaling. At the postsynaptic site, each horizontal and bipolar cell type could individually further widen or reduce the cone photoreceptor provided dynamic range depending on postsynaptic mechanisms (e.g., at the ground squirrel cone photoreceptor to c2b OFF bipolar cell synapse, the dynamic range of the signaling is reduced by AMPA receptor saturation to improve temporal performance; Grabner et al., 2016). Our results indicate that cone photoreceptor HVA L-type channels "piggyback" on LVA T-type Ca^{2+} channels, meaning that depolarization at light offset activates first LVA T-type Ca^{2+} channels, which further activates HVA L-type Ca^{2+} channels. Therefore, the presence of LVA T-type Ca^{2+} channels moves the Ca^{2+} current activation level to more negative potentials where the dark-produced V_m change could already evoke Ca^{2+} influx and synaptic vesicle release. As a result, LVA T-type Ca^{2+} channels extend the dynamic range of cone photoreceptor signaling by boosting synaptic vesicle release near the dark membrane potential.

References

Adler EM, Augustine GJ, Duffy SN, Charlton MP (1991) Alien intracellular calcium chelators attenuate neurotransmitter release at the squid giant synapse. J Neurosci 11:1496–1507.

Akopian A, Witkovsky P (1996) D2 dopamine receptor-mediated inhibition of a hyperpolarization-activated current in rod photoreceptors. J Neurophysiol 76:1828–1835.

Angstadt JD, Calabrese RL (1991) Calcium currents and graded synaptic transmission between heart interneurons of the leech. J Neurosci 11:746–759.

Babai N, Sendelbeck A, Regus-Leidig H, Fuchs M, Mertins J, Reim K, Brose N, Feigenspan A, Brandstätter JH (2016) Functional roles of complexin 3 and complexin 4 at mouse photoreceptor ribbon synapses. J Neurosci 36:6651–6667.

Babai N, Gierke K, Müller T, Regus-Leidig H, Brandstätter JH, Feigenspan A (2019) Signal transmission at invaginating cone photoreceptor synaptic contacts following deletion of the presynaptic cytomatrix protein Bassoon in mouse retina. Acta Physiol (Oxf) 226:e13241.

Bader CR, Bertrand D, Schwartz EA (1982) Voltage-activated and calcium-activated currents studied in solitary rod inner segments from the salamander retina. J Physiol 331:253–284.

Barnes S (1994) After transduction - response shaping and control of transmission by ion channels of the photoreceptor inner segment. Neuroscience 58:447–459.

Barnes S, Hille B (1989) Ionic channels of the inner segment of tiger salamander cone photoreceptors. J Gen Physiol 94:719–743.

Bartoletti TM, Jackman SL, Babai N, Mercer AJ, Kramer RH, Thoreson WB (2011) Release from the cone ribbon synapse under bright light conditions can be controlled by the opening of only a few Ca^{2+} channels. J Neurophysiol 106:2922–2935.

Baylor DA, Nunn BJ, Schnapf JL (1987) Spectral sensitivity of cones of the monkey Macaca-fascicularis. J Physiol 390:145–160.

Bean BP (2007) The action potential in mammalian central neurons. Nat Rev Neurosci 8:451–465.

Bradley JE, Anderson UA, Woolsey SM, Thornbury KD, McHale NG, Hollywood MA (2004) Characterization of T-type calcium current and

its contribution to electrical activity in rabbit urethra. Am J Physiol Cell Physiol 286:C1078–C1088.

Bryman GS, Liu A, Do MTH (2020) Optimized signal flow through photoreceptors supports the high-acuity vision of primates. Neuron 108:335–348.e7.

Cao LH, Luo DG, Yau KW (2014) Light responses of primate and other mammalian cones. Proc Natl Acad Sci U|S|A 111:2752–2757.

Casillas-Espinosa PM, Hicks A, Jeffreys A, Snutch TP, O'Brien TJ, Powell KL (2015) Z944, a novel selective T-type calcium channel antagonist delays the progression of seizures in the amygdala kindling model. PLoS One 10:e0130012.

Cho S, von Gersdorff H (2014) Proton-mediated block of Ca^{2+} channels during multivesicular release regulates short-term plasticity at an auditory hair cell synapse. J Neurosci 34:15877–15887.

Choi SY, Jackman S, Thoreson WB, Kramer RH (2008) Light regulation of Ca2+ in the cone photoreceptor synaptic terminal. Vis Neurosci 25:693–700.

Coulter DA, Huguenard JR, Prince DA (1989) Characterization of ethosuximide reduction of low-threshold calcium current in thalamic neurons. Ann Neurol 25:582–593.

Curtis LB, Doneske B, Liu XQ, Thaller C, Mcnew JA, Janz R (2008) Syntaxin 3b is a t-SNARE specific for ribbon synapses of the retina. J Comp Neurol 510:550–559.

Dib-Hajj SD, Black JA, Waxman SG (2015) $Na_v1.9$: a sodium channel linked to human pain. Nat Rev Neurosci 16:511–519.

Dieck ST, Altrock WD, Kessels MM, Qualmann B, Regus H, Brauner D, Fejtová A, Bracko O, Gundelfinger ED, Brandstätter JH (2005) Molecular dissection of the photoreceptor ribbon synapse: physical interaction of Bassoon and RIBEYE is essential for the assembly of the ribbon complex. J Cell Biol 168:825–836.

Ertel SI, Ertel EA, Clozel JP (1997) T-type Ca^{2+} channels and pharmacological blockade: potential pathophysiological relevance. Cardiovasc Drugs Ther 11:723–739.

Fain GL, Gerschenfeld HM, Quandt FN (1980) Calcium spikes in toad rods. J Physiol 303:495–513.

Feigenspan A, Babai N (2015) Functional properties of spontaneous excitatory currents and encoding of light/dark transitions in horizontal cells of the mouse retina. Eur J Neurosci 42:2615–2632.

Feigenspan A, Babai NZ (2017) Preparation of horizontal slices of adult mouse retina for electrophysiological studies. J Vis Exp (119):55173.

Feigenspan A, Ohs A, von Wittgenstein J, Brandstätter JH, Babai N (2020) Analysis of tetrodotoxin-sensitive sodium and low voltage-activated calcium channels in developing mouse retinal horizontal cells. Exp Eye Res 195:108028.

Feodorova Y, Koch M, Bultman S, Michalakis S, Solovei I (2015) Quick and reliable method for retina dissociation and separation of rod photoreceptor perikarya from adult mice. MethodsX 2:39–46.

Fuchs M, Brandstätter JH, Regus-Leidig H (2014) Evidence for a clathrin-independent mode of endocytosis at a continuously active sensory synapse. Front Cell Neurosci 8:60.

Gayet-Primo J, Yaeger DB, Khanjian RA, Puthussery T (2018) Heteromeric $K_V2/K_V8.2$ channels mediate delayed rectifier potassium currents in primate photoreceptors. J Neurosci 38:3414–3427.

Gee KR, Brown KA, Chen WN, Bishop-Stewart J, Gray D, Johnson I (2000) Chemical and physiological characterization of fluo-4 Ca^{2+}-indicator dyes. Cell Calcium 27:97–106.

Gerschenfeld HM, Piccolino M, Neyton J (1980) Feed-back modulation of cone synapses by L-horizontal cells of turtle retina. J Exp Biol 89:177–192.

Gong S, Zheng C, Doughty ML, Losos K, Didkovsky N, Schambra UB, Nowak NJ, Joyner A, Leblanc G, Hatten ME, Heintz N (2003) A gene expression atlas of the central nervous system based on bacterial artificial chromosomes. Nature 425:917–925.

Grabner CP, Ratliff CP, Light AC, DeVries SH (2016) Mechanism of high-frequency signaling at a depressing ribbon synapse. Neuron 91:133–145.

Grassmeyer JJ, Cahill AL, Hays CL, Barta C, Quadros RM, Gurumurthy CB, Thoreson WB (2019) Ca^{2+} sensor synaptotagmin-1 mediates exocytosis in mammalian photoreceptors. Elife 8:e45946.

Heady TN, Gomora JC, Macdonald TL, Perez-Reyes E (2001) Molecular pharmacology of T-type Ca2+ channels. Jpn J Pharmacol 85:339–350.

Henderson D, Miller RF (2007) Low-voltage activated calcium currents in ganglion cells of the tiger salamander retina: experiment and simulation. Vis Neurosci 24:37–51.

Herzog RI, Cummins TR, Waxman SG (2001) Persistent TTX-resistant Na+ current affects resting potential and response to depolarization in simulated spinal sensory neurons. J Neurophysiol 86:1351–1364.

Hirano AA, Liu X, Boulter J, Grove J, Perez de Sevilla Muller L, Barnes S, Brecha NC (2016) Targeted deletion of vesicular GABA transporter from retinal horizontal cells eliminates feedback modulation of photoreceptor calcium channels. eNeuro 3:ENEURO.0148-15.2016–0115.2016.

Hobai IA, Hancox JC, Levi AJ (2000) Inhibition by nickel of the L-type Ca channel in guinea pig ventricular myocytes and effect of internal cAMP. Am J Physiol Heart Circ Physiol 279:H692–H701.

Hodgkin AL, Huxley AF (1952) A quantitative description of membrane current and its application to conduction and excitation in nerve. J Physiol 117:500–544.

Hu C, Bi A, Pan ZH (2009) Differential expression of three T-type calcium channels in retinal bipolar cells in rats. Vis Neurosci 26:177–187.

Huguenard JR (1996) Low-threshold calcium currents in central nervous system neurons. Annu Rev Physiol 58:329–348.

Ingram NT, Sampath AP, Fain GL (2020) Membrane conductances of mouse cone photoreceptors. J Gen Physiol 152:e201912520.

Iyer R, Ungless MA, Faisal AA (2017) Calcium-activated SK channels control firing regularity by modulating sodium channel availability in midbrain dopamine neurons. Sci Rep 7:5248.

Kaneko A, Tachibana M (1986) Blocking effects of cobalt and related ions on the gamma-aminobutyric acid-induced current in turtle retinal cones. J Physiol 373:463–479.

Kaneko A, Pinto LH, Tachibana M (1989) Transient calcium current of retinal bipolar cells of the mouse. J Physiol 410:613–629.

Kang HW, Park JY, Jeong SW, Kim JA, Moon HJ, Perez-Reyes E, Lee JH (2006) A molecular determinant of nickel inhibition in $Ca_v3.2$ T-type calcium channels. J Biol Chem 281:4823–4830.

Kawai F, Horiguchi M, Suzuki H, Miyachi E (2001) Na+ action potentials in human photoreceptors. Neuron 30:451–458.

Kawai F, Horiguchi M, Ichinose H, Ohkuma M, Isobe R, Miyachi EI (2005) Suppression by an h current of spontaneous Na+ action potentials in human cone and rod photoreceptors. Invest Ophthalmol Vis Sci 46:390–397.

Kersten FF, van Wijk E, van Reeuwijk J, van der Zwaag B, Märker T, Peters TA, Katsanis N, Wolfrum U, Keunen JE, Roepman R, Kremer H (2010) Association of whirlin with Cav1.3 (alpha1D) channels in photoreceptors, defining a novel member of the usher protein network. Invest Ophthalmol Vis Sci 51:2338–2346.

Klöckner U, Lee JH, Cribbs LL, Daud A, Hescheler J, Pereverzev A, Perez-Reyes E, Schneider T (1999) Comparison of the Ca^2+ currents induced by expression of three cloned α1 subunits, α1G, α1H and α1I, of low-voltage-activated T-type Ca^2+ channels. Eur J Neurosci 11:4171–4178.

Koso H, Minami C, Tabata Y, Inoue M, Sasaki E, Satoh S, Watanabe S (2009) CD73, a novel cell surface antigen that characterizes retinal photoreceptor precursor cells. Invest Ophthalmol Vis Sci 50:5411–5418.

Landgraf I, Mühlhans J, Dedek K, Reim K, Brandstätter JH, Ammermüller J (2012) The absence of complexin 3 and complexin 4 differentially impacts the ON and OFF pathways in mouse retina. Eur J Neurosci 36:2470–2481.

Lasater EM, Witkovsky P (1991) The calcium current of turtle cone photoreceptor axon terminals. Neurosci Res Suppl 15:S165–S173.

Lasater EM, Normann RA, Kolb H (1989) Signal integration at the pedicle of turtle cone photoreceptors: an anatomical and electrophysiological study. Vis Neurosci 2:553–564.

Lee JH, Gomora JC, Cribbs LL, Perez-Reyes E (1999) Nickel block of three cloned T-type calcium channels: low concentrations selectively block alpha1H. Biophys J 77:3034–3042.

Lee JH, Kim EG, Park BG, Kim KH, Cha SK, Kong ID, Lee JW, Jeong SW (2002) Identification of T-type alpha1H Ca2+ channels (Ca(v)3.2) in major pelvic ganglion neurons. J Neurophysiol 87:2844–2850.

Lee TS, Kaku T, Takebayashi S, Uchino T, Miyamoto S, Hadama T, Perez-Reyes E, Ono K (2006) Actions of mibefradil, efonidipine and nifedipine block of recombinant T- and L-type Ca channels with distinct inhibitory mechanisms. Pharmacology 78:11–20.

Leuranguer V, Mangoni ME, Nargeot J, Richard S (2001) Inhibition of T-type and L-type calcium channels by mibefradil: physiologic and

pharmacologic bases of cardiovascular effects. J Cardiovasc Pharmacol 37:649–661.

Levic S, Dulon D (2012) The temporal characteristics of Ca2+ entry through L-type and T-type Ca2+ channels shape exocytosis efficiency in chick auditory hair cells during development. J Neurophysiol 108:3116–3123.

Lin ZX, Santos S, Padilla K, Printzenhoff D, Castle NA (2016) Biophysical and pharmacological characterization of Nav1.9 voltage dependent sodium channels stably expressed in HEK-293 cells. PLoS One 11: e0161450.

Macosko EZ, Basu A, Satija R, Nemesh J, Shekhar K, Goldman M, Tirosh I, Bialas AR, Kamitaki N, Martersteck EM, Trombetta JJ, Weitz DA, Sanes JR, Shalek AK, Regev A, McCarroll SA (2015) Highly parallel genome-wide expression profiling of individual cells using nanoliter droplets. Cell 161:1202–1214.

Mansergh F, Orton NC, Vessey JP, Lalonde MR, Stell WK, Tremblay F, Barnes S, Rancourt DE, Bech-Hansen NT (2005) Mutation of the calcium channel gene Cacna1f disrupts calcium signaling, synaptic transmission and cellular organization in mouse retina. Hum Mol Genet 14:3035–3046.

Maricq AV, Korenbrot JI (1988) Calcium and calcium-dependent chloride currents generate action potentials in solitary cone photoreceptors. Neuron 1:503–515.

Maricq AV, Korenbrot JI (1990) Inward rectification in the inner segment of single retinal cone photoreceptors. J Neurophysiol 64:1917–1928.

Martin RL, Lee JH, Cribbs LL, Perez-Reyes E, Hanck DA (2000) Mibefradil block of cloned T-type calcium channels. J Pharmacol Exp Ther 295:302–308.

Masland RH (2012) The neuronal organization of the retina. Neuron 76:266–280.

McFarlane MB, Gilly WF (1998) State-dependent nickel block of a high-voltage-activated neuronal calcium channel. J Neurophysiol 80:1678–1685.

Mercer AJ, Thoreson WB (2011) The dynamic architecture of photoreceptor ribbon synapses: cytoskeletal, extracellular matrix, and intramembrane proteins. Vis Neurosci 28:453–471.

Mercer AJ, Chen MH, Thoreson WB (2011) Lateral mobility of presynaptic L-type calcium channels at photoreceptor ribbon synapses. J Neurosci 31:4397–4406.

Morgans CW (1999) Calcium channel heterogeneity among cone photoreceptors in the tree shrew retina. Eur J Neurosci 11:2989–2993.

Morgans CW (2001) Localization of the alpha(1F) calcium channel subunit in the rat retina. Invest Ophthalmol Vis Sci 42:2414–2418.

Morgans CW, Gaughwin P, Maleszka R (2001) Expression of the alpha1F calcium channel subunit by photoreceptors in the rat retina. Mol Vis 7:202–209.

Morgans CW, Brandstätter JH, Kellerman J, Betz H, Wässle H (1996) A SNARE complex containing syntaxin 3 is present in ribbon synapses of the retina. J Neurosci 16:6713–6721.

Morgans CW, Bayley PR, Oesch NW, Ren GY, Akileswaran L, Taylor WR (2005) Photoreceptor calcium channels: insight from night blindness. Vis Neurosci 22:561–568.

Nachman-Clewner M, St Jules R, Townes-Anderson E (1999) L-type calcium channels in the photoreceptor ribbon synapse: localization and role in plasticity. J Comp Neurol 415:1–16.

Nelson MT, Joksovic PM, Su P, Kang HW, Van Deusen A, Baumgart JP, David LS, Snutch TP, Barrett PQ, Lee JH, Zorumski CF, Perez-Reyes E, Todorovic SM (2007) Molecular mechanisms of subtype-specific inhibition of neuronal T-type calcium channels by ascorbate. J Neurosci 27:12577–12583.

O'Brien BJ, Caldwell JH, Ehring GR, O'Brien KMB, Luo SJ, Levinson SR (2008) Tetrodotoxin-resistant voltage-gated sodium channels Na(v)1.8 and Na(v)1.9 are expressed in the retina. J Comp Neurol 508:940–951.

Oltedal L, Veruki ML, Hartveit E (2009) Passive membrane properties and electrotonic signal processing in retinal rod bipolar cells. J Physiol 587:829–849.

Osorio N, Korogod S, Delmas P (2014) Specialized functions of Nav1.5 and Nav1.9 channels in electrogenesis of myenteric neurons in intact mouse ganglia. J Neurosci 34:5233–5244.

Pan ZH (2000) Differential expression of high- and two types of low-voltage-activated calcium currents in rod and cone bipolar cells of the rat retina. J Neurophysiol 83:513–527.

Pan ZH, Hu HJ, Perring P, Andrade R (2001) T-type Ca(2+) channels mediate neurotransmitter release in retinal bipolar cells. Neuron 32:89–98.

Perez-Reyes E (2003) Molecular physiology of low-voltage-activated t-type calcium channels. Physiol Rev 83:117–161.

Perez-Reyes E, Cribbs LL, Daud A, Lacerda AE, Barclay J, Williamson MP, Fox M, Rees M, Lee JH (1998) Molecular characterization of a neuronal low-voltage-activated T-type calcium channel. Nature 391:896–900.

Protti DA, Flores-Herr N, von Gersdorff H (2000) Light evokes Ca2+ spikes in the axon terminal of a retinal bipolar cell. Neuron 25:215–227.

Regus-Leidig H, Ott C, Löhner M, Atorf J, Fuchs M, Sedmak T, Kremers J, Fejtová A, Gundelfinger ED, Brandstätter JH (2013) Identification and immunocytochemical characterization of Piccolino, a novel Piccolo splice variant selectively expressed at sensory ribbon synapses of the eye and ear. PloS one 8:e70373.

Regus-Leidig H, Atorf J, Feigenspan A, Kremers J, Maw MA, Brandstätter JH (2014a) Photoreceptor degeneration in two mouse models for congenital stationary night blindness type 2. PLoS One 9:e86769.

Regus-Leidig H, Fuchs M, Löhner M, Leist SR, Leal-Ortiz S, Chiodo VA, Hauswirth WW, Garner CC, Brandstätter JH (2014b) In vivo knockdown of Piccolino disrupts presynaptic ribbon morphology in mouse photoreceptor synapses. Front Cell Neurosci 8:259.

Reim K, Wegmeyer H, Brandstätter JH, Xue MS, Rosenmund C, Dresbach T, Hofmann K, Brose N (2005) Structurally and functionally unique complexins at retinal ribbon synapses. J Cell Biol 169:669–680.

Reim K, Regus-Leidig H, Ammermüller J, El-Kordi A, Radyushkin K, Ehrenreich H, Brandstätter JH, Brose N (2009) Aberrant function and structure of retinal ribbon synapses in the absence of complexin 3 and complexin 4. J Cell Sci 122:1352–1361.

Rieke F, Schwartz EA (1994) A cGMP-gated current can control exocytosis at cone synapses. Neuron 13:863–873.

Schnapf JL, Kraft TW, Baylor DA (1987) Spectral sensitivity of human cone photoreceptors. Nature 325:439–441.

Schnapf JL, Nunn BJ, Meister M, Baylor DA (1990) Visual transduction in cones of the monkey macaca-fascicularis. J Physiol 427:681–713.

Schneeweis DM, Schnapf JL (1995) Photovoltage of rods and cones in the macaque retina. Science 268:1053–1056.

Solovei I, Kreysing M, Lanctôt C, Kösem S, Peichl L, Cremer T, Guck J, Joffe B (2009) Nuclear architecture of rod photoreceptor cells adapts to vision in mammalian evolution. Cell 137:356–368.

Specht D, Wu SB, Turner P, Dearden P, Koentgen F, Wolfrum U, Maw M, Brandstätter JH, tom Dieck S (2009) Effects of presynaptic mutations on a postsynaptic Cacna1s calcium channel colocalized with mGluR6 at mouse photoreceptor ribbon synapses. Invest Ophthalmol Vis Sci 50:505–515.

Stengel W, Jainz M, Andreas K (1998) Different potencies of dihydropyridine derivatives in blocking T-type but not L-type Ca2+ channels in neuroblastoma-glioma hybrid cells. Eur J Pharmacol 342:339–345.

Strom TM, Nyakatura G, Apfelstedt-Sylla E, Hellebrand H, Lorenz B, Weber BHF, Wutz K, Gutwillinger N, Rüther K, Drescher B, Sauer C, Zrenner E, Meitinger T, Rosenthal A, Meindl A (1998) An L-type calcium-channel gene mutated in incomplete X-linked congenital stationary night blindness. Nat Genet 19:260–263.

Talbot MJ, Sayer RJ (1996) Intracellular QX-314 inhibits calcium currents in hippocampal CA1 pyramidal neurons. J Neurophysiol 76:2120–2124.

Tang AH, Karson MA, Nagode DA, McIntosh JM, Uebele VN, Renger JJ, Klugmann M, Milner TA, Alger BE (2011) Nerve terminal nicotinic acetylcholine receptors initiate quantal GABA release from perisomatic interneurons by activating axonal T-type (Ca_v3) Ca^{2+} channels and Ca^{2+} release from stores. J Neurosci 31:13546–13561.

Tang CM, Presser F, Morad M (1988) Amiloride selectively blocks the low threshold (T) calcium channel. Science 240:213–215.

Taylor WR, Morgans C (1998) Localization and properties of voltage-gated calcium channels in cone photoreceptors of Tupaia belangeri. Vis Neurosci 15:541–552.

To KHT, Gui PC, Li M, Zawieja SD, Castorena-Gonzalez JA, Davis MJ (2020) T-type, but not L-type, voltage-gated calcium channels are dispensable for lymphatic pacemaking and spontaneous contractions. Sci Rep 10:70.

Van Hook MJ, Nawy S, Thoreson WB (2019) Voltage- and calcium-gated ion channels of neurons in the vertebrate retina. Prog Retin Eye Res 72:100760.

Vignali S, Leiss V, Karl R, Hofmann F, Welling A (2006) Characterization of voltage-dependent sodium and calcium channels in mouse pancreatic A- and B-cells. J Physiol 572:691–706.

Wilkinson MF, Barnes S (1996) The dihydropyridine-sensitive calcium channel subtype in cone photoreceptors. J Gen Physiol 107:621–630.

Wu J, Marmorstein AD, Striessnig J, Peachey NS (2007) Voltage-dependent calcium channel CaV1.3 subunits regulate the light peak of the electroretinogram. J Neurophysiol 97:3731–3735.

Xiao HL, Chen XM, Steele EC (2007) Abundant L-type calcium channel $Ca_v1.3$ (α1D) subunit mRNA is detected in rod photoreceptors of the mouse retina via in situ. Molecular Vision 13:764–771.

Xu JW, Slaughter MM (2005) Large-conductance calcium-activated potassium channels facilitate transmitter release in salamander rod synapse. J Neurosci 25:7660–7668.

Yagi T, Macleish PR (1994) Ionic conductances of monkey solitary cone inner segments. J Neurophysiol 71:656–665.

Zamponi GW, Bourinet E, Snutch TP (1996) Nickel block of a family of neuronal calcium channels: subtype- and subunit-dependent action at multiple sites. J Membr Biol 151:77–90.

Zanetti L, Kilicarslan I, Netzer M, Babai N, Seitter H, Koschak A (2021) Function of cone and cone-related pathways in $Ca_V1.4$ IT mice. Sci Rep 11:2732.